EUROPEAN ORGANIZATION FOR NUCLEAR RESEARCH

CERN-PPE / 93-23
February 11, 1993

FURTHER RESULTS ON CERIUM FLUORIDE CRYSTALS

the Crystal Clear Collaboration

ABSTRACT

A systematic investigation of the properties of Cerium Fluoride monocrystals has been performed by the "Crystal Clear" collaboration in view of a possible use of such crystals for the construction of high precision electromagnetic calorimeters for the future generation of high luminosity accelerators. A large sample of different crystals grown by several producers has been studied. The spectroscopic characteristics, the transmission, luminescence and excitation spectra and the decay time curves are analysed. The light yield of the different crystals is measured with photomultipliers and Si photodiodes and compared to reference standards like BGO and NaI(Tl). The radiation damage behaviour is then presented for γ and neutron irradiations, at different doses and dose rates, including thermal and optical bleaching.

Submitted to Nuclear Instruments and Methods

S. Anderson[12], E. Auffray[1], T. Aziz[15], S. Baccaro[5], S. Banerjee[15], P. Bareyre[2], L.E. Barone[4], B. Borgia[4], D. Boutet[11], J.P. Burq[8], M. Chemarin[8], R. Chipaux[2], I. Dafinei[1], P. D'Atanasio[5], F. De Notaristefani[4], B. Dezillie[1], C. Dujardin[11], S. Dutta[15], J.L. Faure[2], J . Fay[8], D. Ferrère[9], O.P. Francescangeli[3], B.A. Fuchs[10], S.N. Ganguli[15], G. Gillespie[10], M. Goyot[8], S.K. Gupta[15], A. Gurtu[15], J. Heck[10], A. Hervé[1], H. Hillemanns[14], F. Holdener[10], B. Ille[8], L. Jönsson[12], J Kierstead[16], W. Krenz[14], W. Kway[10], J.M. Le Goff[1], M. Lebeau[9], P. Lebrun[8], P. Lecoq[1], Y. Lemoigne[2], G. Loomis[10], K. Lubelsmeyer[14], N. Madjar[8], G. Majni[3], H. El Mamouni[8], S. Mangla[15], J.A. Mares[7], J.P Martin[8], M. Mattioli[4], G.J. Mauger[10], K. Mazumdar[15], P.F. Mengucci[3], J.P. Merlo[2], B. Moine[11], N. Nikl[7], J.P. Pansart[2], C. Pedrini[11], J. Poinsignon[2], K. Polak[7], R. Raghavan[15], P. Rebourgeard[2], D.T. Rinaldi[3], J. Rosa[7], A. Rosowsky[2], P. Sahuc[8], V. Samsonov[13], S. Sarkar[15], V. Schegelski[13], D. Schmitz[14], M. Schneegans[9], D. Seliverstov[13], S. Stoll[16], K. Sudhakar[15], A. Svensson[12], S.C. Tonwar[15], V. Topa[6], J.P. Vialle[9], M. Vivargent[9], W. Wallraff[14], M.J. Weber[10], N. Winter[10], C. Woody[16], C.R. Wuest[10], V. Yanovski[13].

[1] *CERN Geneva, Switzerland*
[2] *DAPNIA Saclay, France*
[3] *INFN Ancona, Italy*
[4] *INFN Rome, Italy*
[5] *ENEA Casaccia, INFN Rome, Italy*
[6] *Institute of Atomic Physics (IFA) ,Bucharest, Romania*
[7] *Institute of Physics, Praha, Czech Repbublic*
[8] *IPN of Lyon, IN2P3-CNRS and Université Claude Bernard, Villeurbanne, France*
[9] *LAPP, IN2P3-CNRS, Annecy-le-Vieux ,France*
[10] *Laurence Livermore National Laboratory, USA*
[11] *LPCML of Lyon, CNRS and Université Claude Bernard, Villeurbanne, France*
[12] *Lund University, Sweden*
[13] *Petersburg Nuclear Physics Institute, St-Petersburg, CIS*
[14] *Physics Institute, RWTH Aachen, Germany*
[15] *Tata Institute of Fundamental Research, Bombay, India*
[16] *Brookhaven National Laboratotory, USA,* Not a member of the Crystal Clear Collaboration

Submitted to Nuclear Instruments and Methods

1. Introduction:

The quest for a new generation of dense, fast and radiation hard scintillators has become very active in the last few years due to an increasing demand for high resolution gamma calorimetry and imaging in various fields like astrophysics, medicine, nuclear and high energy physics, oil well logging and ore sorting, as well as security and inspection systems. For several of these applications, the constraints in terms of event rates and radiation levels are extremely severe, particularly for high energy physics at the new generation of high luminosity accelerators (LHC, SSC, factories) [1].

Cerium Fluoride (CeF3) has been recently identified as a good scintillator candidate for high rate calorimetry [2,3]. The reasons are a high density of this crystal, 6.16g/cm^3, due to the compactness of the lattice (the density of Ce^{3+} ions is as large as 1.88×10^{22} cm^{-3}), which yields a small radiation length (1.68cm) and a very small Molière radius (2.6cm), and a fast luminescence in the near UV without afterglow. A negligible temperature coefficient of the light emission (0.1%/°C at room temperature) is also an attractive property for the design of detectors requiring a very high stability over periods of several months or years.

In the general context of a large R&D effort to prepare the detector technologies for the future experiments in high energy physics the Crystal Clear Collaboration [4] has undertaken a more precise evaluation of the properties of CeF3. More than 20 crystals grown by five different manufacturers have been systematically tested from the point of view of their spectroscopic and radiation resistance characteristics. It must be said that there is a rapidly growing interest for this crystal and that more companies are becoming active in this field. This report gives a summary of the main results obtained so far. The different optical spectra (transmission, excitation, photo and radio-luminescence) are compared for all the crystals as well as the kinetic of their luminescence. Explanations are given in the frame of a model to describe the luminescence mechanism of CeF3. An analysis of the light yield of the different samples is made as a function of known characteristics of these crystals. A systematic investigation of the gamma and neutron radiation effects is then presented for several accumulated doses and dose rates. The recovery as a function of time, temperature and light illumination is also shown, and an analysis of factors influencing the radiation resistance of CeF3 is discussed.

2. Experimental conditions:

2.1 Crystal samples

The list of the 22 crystals used for this study and produced by 5 different companies is given in Table 1 together with their principal characteristics. Some of the samples have been cut from different places of

the same 20cm long ingot. The dimensions of the crystals differ from sample to sample, but the cross section is at least 1cm^2 to allow for a good optical transmission measurement and the length ranges from 1cm to 11cm which gives enough sensitivity for the bulk absorption. It is to be noticed that a few crystals have been doped with Barium which seems to decrease the number of scattering centres in the crystal [3,5] and has been reported to increase the radiation tolerance [6].

Name	Producer	Dimensions (mm^3)	Comments
CF 04	Optovac (USA)	10x10x10	Undoped
CF 05	Optovac (USA)	10x10x10	Undoped
CF 30	Optovac (USA)	20x20x78	From ingot 1 (10cm) Poor raw material (200ppm Nd)
CF128	Optovac (USA)	18x17x9	From ingot 2 (20 cm) Pure raw material
CF 130	Optovac (USA)	17x17x28	From ingot 2 (20 cm) Pure raw material
CF 169	Optovac (USA)	21x21x15.5	From ingot 2 (20 cm) Pure raw material
CF 171	Optovac (USA)	20x20x110	From ingot 3 (20 cm) Oxygen contamination
CF 186	Optovac (USA)	20x20x74	From ingot 4 (20 cm) Oxygen contamination
CF 204	Optovac (USA)	15x20x76	0.5% Ba doped From ingot 5 (20cm)
CF 205	Optovac (USA)	15x20x30	0.5% Ba doped From ingot 5 (20cm)
CF 238	Optovac (USA)	18x20x50	0.5% Ba doped From ingot 6 (20cm)
CF 239	Optovac (USA)	15x20x30	0.5% Ba doped From ingot 6 (20cm)
CF 278	Optovac (USA)	Ø32x85	0.5% Ba doped From ingot 7 (20cm)
CF 202	NKK (Japan)	15x20x55	Undoped
CF 166	Shanghai institute of Ceramics (China)	Ø21x28	Undoped
CF 167	Shanghai institute of Ceramics (China)	Ø22x41	Undoped
CF 185	Vavilov St.Opt.Inst Saint Petersbourg (Russia)	Ø11.5x40.5	Ba doped Concentration unknown
CF 207	Preciosa Monokrystaly Turnov (Czech Republic)	14x20x30	Undoped
CF 208	Preciosa Monokrystaly Turnov (Czech Republic)	14x20x30	Undoped
CF 214	Preciosa Monokrystaly Turnov (Czech Republic)	8.3x10x33	Undoped
CF 215	Preciosa Monokrystaly Turnov (Czech Republic)	9.6x20x26,2	Undoped
CF 306	Preciosa Monokrystaly Turnov (Czech Republic)	10x10x10	Undoped

Table 1 : List of 22 tested crystals

2.2 Optical transmission measurements

The optical transmission spectra of crystals before and after irradiation were obtained in the range of 200 to 700nm on a spectrophotometer built at CERN, using a 150W Xenon lamp as a source and a Jobin-Yvon H20UV monochromator with a resolution of 2nm. For the neutron irradiation tests in Bombay a commercial double beam spectrophotometer Shimadzu UV2100 was used. Measurements at Brookhaven and ENEA Rome, were performed respectively on a model Hitachi 3210 and a double beam Perkin-Elmer 340 spectrophotometer.

When comparing crystals before and after irradiation it is often useful to calculate the radiation induced absorption coefficient from the optical transmission measurements:

$$\mu = (1/L) \times \mathrm{Ln}\,(T_0/T)$$

where μ: is the absorption coefficient
T_0: is the initial optical transmission before irradiation
T: is the optical transmission after irradiation
L: is the crystal length in meters

2.3 Fluorescence measurements

Excitation and emission spectra were recorded on a spectrofluorimeter model JY3D (Jobin-Yvon) built around 2 monochromators H20UV with a resolution of 2nm. The UV synchrotron radiation from the SUPERACO storage ring at LURE (Orsay, France) with a 3 meter vacuum-UV monochromator was also used as a light source.

2.4 Decay time spectra

The fluorescence decay time was measured using the delayed coincidence method [7]. A β^+ Na^{22} source excites both a fast plastic scintillator and the crystal. The delayed signal from the plastic scintillator coupled to a photomultiplier tube gives the stop signal, and a second photomultiplier tube (Philips XP2020Q) placed at 10cm from the scintillator crystal and working in the single photon mode gives the start signal. The signals are processed through constant fraction discriminators and a time to amplitude converter Ortec 566 and recorded on a Tracor-Northern TN-7200 multichannel analyser.

2.5 Light yield measurements

The light yield (LY) measurements quoted in this paper refer in fact to the amount of light collected, i.e. extracted from the crystal and impinging on the photo-cathode of a photomultiplier or on the sensitive area of a photodiode. The samples used are in general large enough to fully contain the photon energy, but remain in most cases squat objects shorter than 8cm. No attempt has been made to correct for sample shape or

volume. For these measurements, the crystals are wrapped with a 12μm thick reflective sheet of aluminized mylar and optically coupled to a quartz window XP2020Q Philips photomultiplier (PM) by an optical oil 47V Rhodorsil from Rhône-Poulenc. The fluorescence produced by gamma rays from a Cs^{137} radioactive source is measured by the PM and the signal is processed by a shaping amplifier Borer type CERN N2620 and analysed on a Tracor-Northern TN-7200 multichannel analyser.

One of the crystal samples (CF130) has been also readout by commercial photodiodes (PD) and the LY measured in a cosmic ray set-up. Two "equivalent" types of commercial UV PIN PD were used: one was provided by Hamamatsu (1725-05 type, $1cm^2$ active area, capacitance of ~$100pf/cm^2$ at 40V) and one from AME (AE 987-1, $1cm^2$, capacitance of ~$40pf/cm^2$). Both types have a UV window made of fused silica or saphire which protects the anode bonding of the PD, thus including a thin layer of air between the entrance window and the diode itself, causing light losses due to total reflection. For these measurements, the crystal was wrapped in one layer of "Millipore" paper and 2 PDs of the same type were connected in parallel to a charge sensitive preamplifier, the output of which was shaped and amplified in an ORTEC 872 amplifier (t = 2μsec). The signals were then analysed in coincidence with the pulses of 2 scintillator counters.

2.6 Irradiation sources

The cerium fluoride crystals were irradiated with the Co^{60} source (4400Ci) from the radiotherapy unit of Geneva Cantonal Hospital, in 250Gy dose steps with 24 hours breaks between steps up to a total dose of 1250Gy. One sample (CF278) was irradiated in air at room temperature at the Cobalt source of the Brookhaven National Laboratory, USA, at increasing doses up to 35kGy and 2 other crystals (CF239 and CF306) at the Cobalt source Calliope at ENEA near Rome, Italy, at a dose rate of 1.105Gy/sec up to 102kGy. Low dose rate measurements were performed on sample CF128 using the 680 mCi Cobalt source (1.2Gy/hour) of the DEIN of the CE Saclay, France.

For neutron irradiations, samples CF04 and CF05 were irradiated in a uniform neutron flux inside the 300kW swimming pool nuclear reactor APSARA at the Bhabha Atomic Research Centre in Bombay, India. A cadmium column at 47cm from the reactor core provides a fast neutron flux of $10^8 cm^{-2} sec^{-1}$ above 1 MeV. In the irradiation chamber (a water tight aluminium vessel with 2cm thick lead wall) the gamma contamination is small (≤ 7%). The neutron energy spectrum, measured from the induced radioactivity in foils of Fe, Co, Ni, Cu, Mn, In, Ti, Au, irradiated together with the crystals, was found to be similar to what is expected at LHC.

3. Optical properties measurements:

3.1 Optical transmission spectra

Transmission curves are in general similar from crystal to crystal, with an average transmission ranging between 78% and 88% at a wavelength higher than 350nm, depending on the possible presence of scatter centres in the bulk of the crystal and on the quality of the surface polishing. It is to be noticed that from the values of the index of refraction of 1.67 at 350nm and 1.63 at 500nm [8] the maximum transmission to be expected from a perfectly polished crystal without absorption is 88.2% and 89.1% respectively, very close to what has been obtained on the best crystals. The transmission curve reflects the quality of the crystal as illustrated on Fig 1 showing the considerable improvement obtained after a purification process which resulted in a reduction of the neodymium contents in the raw material from 200ppm to 2ppm. Another evidence of the sensitivity of the transmission measurement to impurities or defects is the observation in some crystals of a gradient of the transversal transmission measured in several places along the crystal due to the segregation of impurities during the growth process (Fig 2).

When comparing the different crystals a spread of the transmission band edge position of typically 25nm is observed (Fig 3). The barium doped crystals have a band edge systematically shifted above 300nm (measured at half of the optical transmission value at 700nm), to be compared to about 285nm for our best crystals for light yield and radiation hardness. Several other crystals, grown as pure crystals, have the band edge at intermediate values. For some crystals (CF30) a displacement of the band edge of nearly 10nm has been observed between the two extremities. It is very likely that the band edge position is strongly coupled to the density of fluorine vacancies in the lattice which will change the local crystal field seen by the Ce^{3+} ions. Wanted or accidental doping with a divalent cation like Ba^{2+} will increase this density by offering an easy way for charge compensation of these impurities. A local increase of the crystal field can be produced by these defects which will result in a reduction of the energy gap between the ground state (4f) and first excited state (5d) of the Ce^{3+} ion. A similar effect is observed with calcium and strontium doping [5].

3.2 Luminescence spectra

In order to minimize the self absorption of the CeF3 lattice below 300nm the luminescence spectra were measured on the surface of the samples when excited by a UV light beam at grazing incidence.

Although the photo-luminescence emission spectra are always characterized by several emission bands in the near UV, the relative amplitude of these bands, and sometimes their position show some differences from sample to sample, depending on the producer, crystal growth conditions and doping. We have classified the spectra in three

main categories which are strongly correlated with the absorption band edge position.

When excited at the maximum of their excitation spectrum, the undoped CeF_3 crystals with the larger transmission band (CF169) have two emission bands positioned at 286nm and 305nm and a weaker broad band at 340nm. For the crystals of the intermediate category (CF202) the 286 and 305nm bands are strongly suppressed (partly because of reabsorption due to the band edge shift) and the emission is characterized by a broad band at 335nm with 2 shoulders at 360 and 385nm. For the crystals of these 2 types the 340nm emission peak can be directly excited at about 286nm where the first emission band is located, suggesting a resonant energy transfer between the luminescent centre responsible for the 286nm emission peak and the one responsible for the 340nm peak (Fig 4a and 4b). This fact is also supported by the systematic balance between the amplitudes of the 286nm and the 340nm emission peaks, when the excitation wavelength is varied or when the band edge is shifted at longer wavelength, an effect which cannot be attributed to the reabsorption only (Fig 5).

Barium doped CeF_3 crystals have three more emission peaks positioned at 325nm, 360nm and 385nm which, at 0.5% Ba impurity level, become dominant (Fig 4c). The nature of the luminescent centres responsible for these new emission bands is not yet fully understood but no sign of energy transfer has been observed when varying the excitation wavelength contrary to what is seen on the undoped crystals.

For practical applications in calorimetry it is interesting to measure the luminescence spectrum when excited by γ rays. This was done by analysing the light produced in the sample by a Cs^{137} source with a monochromator and a XP2020Q photomultiplier using a photon counting method. The radio-luminescence spectra obtained for a pure (CF130) and a Ba doped crystal (CF205) are plotted in Fig 6. For the pure crystal the spectrum is rather narrow and peaks at 305nm. The peak at 286nm is not present, as expected from the absorption of the lattice. The 340nm band is only visible as a tail which means either that the efficiency of the energy transfer is smaller, or that the number of luminescent centres for the 340nm emission is smaller in the case of radio-luminescence as compared to photo-luminescence. A possible explanation could be that radio-excitation takes place in the bulk of the crystal, whereas photo-excitation only concerns a small layer near the surface, because of the very strong lattice absorption in the UV. The 340nm emission band could be produced by Ce^{3+} ions perturbed by the vicinity of oxygen ions or fluorine vacancies which have the higher probability to be produced near the surface.

For the Ba doped crystals the radio-luminescence spectrum is much wider and rather similar to the photo-luminescence spectrum with some minor differences in the relative amplitudes of the different bands.

3.3 Excitation spectra

In order to better understand the spectroscopy of CeF3, excitation spectra of mixed crystals LaF3-CeF3 with cerium concentration increasing from 0.05% to 100% have been recorded at low temperature (10°K) using synchrotron radiation (SUPERACO at Orsay, France) as a light source. The choice of LaF3 as a host for Ce^{3+} ions was motivated by the similarity of the crystalline structure of LaF3 and CeF3. It must be said that this study was made on a series of samples grown several years ago by Optovac without optimized processing and raw materials. Nevertheless some interesting observations have been made.

A weakly doped sample (0.05% Ce) exhibits five excitation bands in the 190 to 250nm region, attributed to the transition from the 4f to the 5d level of the Ce^{3+} ion, five times splitted by the crystal field (Fig 7a). Another band at 160nm is assigned to the f $\rightarrow$ s transition. This spectrum reproduces exactly the absorption spectrum on a thin slice. When the cerium concentration increases a similar structure is observed with the addition of a new broad band at longer wavelength around 286nm, which was shown to be involved in the emission around 340nm (Fig 7b). The intensity of both the excitation band at 286nm and the emission band at 340nm increase with the Ce concentration. Moreover, for a given cerium concentration, the intensity of the 340nm emission band increases with temperature [9]. All these data suggest that beside the Ce^{3+} emission at 286 and 300nm there is a trap emission at 340nm with an efficient and thermally assisted Ce^{3+} $\rightarrow$ trap energy transfer. The nature of this trap will be discussed in the next paragraph.

3.4 Decay time

The undoped crystals show a light decay time with 2 regimes, one of about 10nsec and a longer one of typically 30nsec (Fig 8a). The decay time of the doped crystals is non exponential but can be approximated by a component of about 20nsec and another one of about 30nsec (Fig 8b). The dispersion of these parameters from crystal to crystal within each category is very small.

The first decay regime results from the combination to the slow component of 30nsec of another very fast component of a few nsec. The parameters of a 2 exponential fit are listed in table 2 for a few crystals. The amplitude of the fast component represents about 1/3 to 1/2 of the total. However the light yield is dominated by the second component (assuming an infinite gate).

If a monochromator is inserted in the decay time measurement bench this analysis can be done at each wavelength of the emission spectrum. Fig 9a and 9b show the decay time spectra at different wavelengths for one undoped (CF130) and one doped (CF205) crystal respectively. Table 3 gives the fit parameters.

crystal	First component			Second component		
	decay (nsec)	% amplitude	% light yield	decay (nsec)	% amplitude	% light yield
CF130	3	40.0	6.5	32	60.0	93.5
CF169	3	32.0	4.4	32	68.0	95.6
CF202	2	20.0	1.6	32	80.0	98.4
CF185	6.5	54.5	22.0	29	45.5	78.0
CF205	11	52.0	28.0	32	48.0	71.6

Table 2 : Exponential fit to the total light decay time spectra of several crystals

crystal	wavelength (nm)	First component			Second component		
		decay (nsec)	% amplitude	% light yield	decay (nsec)	% amplitude	% light yield
CF130	270	3	49.0	13.3	20.5	51.0	86.7
	275	4	51.7	18.6	21	48.3	81.4
	280	4	48.3	15.7	21	51.7	84.3
	285	4	47.6	15.3	21	52.4	84.7
	290	4	51.5	15.0	22	48.5	85.0
	295	4	51.6	15.6	24	48.4	84.4
	300	5	53.0	19.0	25	47.0	81.0
	305	5	51.6	18.2	26	48.4	81.8
	310	5	49.6	15.9	27	50.4	84.1
	315	5	40.0	10.9	30	60.0	89.1
	320	5	38.7	9.2	32	61.3	90.8
CF205	300	2.5	74.3	33.8	17	25.7	66.2
	320	4	60.9	24.7	20	29.1	75.3
	350	14	52.4	36.1	26	47.6	63.9
	370	14	46.7	27.8	31	53.3	72.2
	400	14	32.6	17.7	32.5	67.4	82.3

Table 3 : Exponential fit to the decay time spectra of one undoped and one doped crystal at different wavelengths

It is important to notice the increase of the decay time of both components when the wavelength increases. Moreover the trap emission at 340nm is characterized by a rise time of about 10nsec (Fig 9a) which supports the idea of an efficient energy transfer from excited Ce^{3+} to traps. The spectroscopic characteristics of Ce^{3+} at normal sites and trap centers being very similar, it is likely that the traps are Ce^{3+} ions occupying perturbed sites giving rise to an inhomogeneously broadened emission band (see § 3.2 and 3.3). The perturbation occurs in the nearest environment of Ce^{3+} ions around the fluorine ions, for instance a F^- vacancy or a O^{2-} ion at the place of one F^- ligand. The nine nearest neighbour F^- ions are situated at various distances to Ce^{3+} explaining the large inhomogeneous broadening of the trap emission band. The longer fluorescence lifetimes of traps can be explained by the λ^2 dependence of

the radiative lifetime of the emitting levels deduced from the Einstein coefficient for the dipole-dipole interaction.

3.5 Light yield

Two methods were used for measuring light yields (LY) with PMs:

a) Calibration of the ADC channels in units of photoelectrons by observation of the single electron peak. The position of the 0.662 MeV peak of Cs^{137} can then be directly expressed in photoelectrons per MeV. This method is in principle safe, but suffers from the uncertainty on channel zero determination, resulting in an error of ~5%. In case of LY comparison with no change in crystal and in HV conditions, direct reading of the peak position in ADC channels can be used yielding a better relative precision.

b) Measurement of the FWHM of the Cs^{137} peak. A LY expressed in number of photoelectrons per MeV can be deduced, but a correction has to be applied for a fixed contribution to the observed width, coming essentially from the variance of the PM gain. This correction has been derived from the 7.5% resolution (FWHM) measured in a NaI(Tl) crystal for which the light contribution to the width is smallest. This value, compared to the LY in NaI(Tl) measured by the first method: 4720 pe/MeV or 21900 photons/MeV, allows to derive the constant contribution. The uncertainty for the second method can be estimated to be ~5%, including the error in deconvoluting the constant term. A correction by a constant contribution of 6.3% yields a very good agreement of both methods for all measurements, with no systematic deviation.

The following results will be given as the mean of both methods, corrected for the PM quantum efficiency at the emission peak wavelength and expressed in number of photons/MeV. The global uncertainty on the LY determination is estimated to be ± 4%.

The light yield of the samples listed in Table 1 was measured with the PM by the 2 methods explained above. The two pure CeF3 samples, produced with good raw materials, gave relatively high LY:

CF130: 1510 photons/MeV CF169: 1400 photons/MeV

CF130, which was never irradiated can be compared to a BGO sample of similar geometry and wrapping, yielding 2760 photons/MeV. Thus, we measure ratios:

$$LY\ (CeF3) = (55 \pm 3)\% \times LY\ (BGO)$$

$$LY\ (CeF3) = (6.9 \pm 0.5)\% \times LY\ (NaI(Tl))$$

Sample CF130 was also measured with the two types of photodiodes mentioned earlier on the cosmic-ray set-up. The electronic chain was carefully characterized and calibrated with low energy γ sources, using the

PD as a detector. The electronic noise for t = 2μsec was typically 950 electrons for the Hamamatsu (C_D = 200pf) and 710 electrons for the AME (C_D = 80pf). For both PDs, a wide peak appears in the pulse height spectrum above the electronic noise corresponding to ~22 MeV deposited in the crystal. Fitting the spectra with the sum of an exponential and a gaussian function, one obtains, after correcting for PD quantum efficiencies (taken from the constructors) and for geometrical matching factor:

1490 photons/MeV for the Hamamatsu PD,

1260 photons/MeV for the AME PD.

The discrepancy between the two values can be due to the uncertainty on the true quantum efficiency of the PDs.

The light of CeF3 sample CF169 was also measured with the PM applying a gate of adjustable length and delay on the linear pulse. The length of the gate was varied between 0 and 100nsec, starting from the bottom of the pulse rise. The response (channel number of peak position minus pedestal), normalized to the ungated signal and plotted ias a function of the gate length is shown in Fig 10. One can see for instance that an integration over 25nsec would yield more than 50% of the total light.

The LY of several CeF3 samples is plotted in Fig 11 as a function of the optical band-edge position defined as the wavelength corresponding to 50% of the transmission value at 700nm. One observes a reduced LY (~50%) for the Ba doped crystals. Samples CF166 and CF167 from SIC have a poor LY (also before irradiation) and CF30 from Optovac shows after irradiation and heating a residual light loss (also seen in transmission). The other data exhibit a clear correlation showing that the red-shift of the band-edge for Ba doped crystals implies a loss of light.

The measured light yield confirms that the energy resolution of a CeF3 calorimeter should not be limited by the photostatistics, at least in the GeV energy range. Moreover readout of CeF3 crystals with Si photodiodes seems possible at the high energy colliders. Nevertheless, theoretical calculations are under way in order to predict the maximum amount of light one might expect from cerium fluoride, in the foreseen geometry.

4. Radiation induced damage:

4.1 General characteristics for aγ irradiation

After a strong gamma irradiation at high dose rate (typically 1000Gy at 250Gy per hour) some crystals produced after an extensive work on the quality of the raw material, like CF169 or CF128, do not show any sign of radiation damage both in optical transmission and in light yield [10]. With the precision of our transmission measurement, this corresponds to an

attenuation length of at least 2m after 1000Gy irradiation (Fig12).

For the other crystals a slight grey coloration appears after irradiation due to the presence of 2 strong absorption bands at 340nm and 385nm. In some cases a third weak and broad band is also visible centred at 540nm. Measurements done at Brookhaven 3 minutes after irradiation show another peak at 620nm decaying away in just a few minutes. The amplitude of these absorption bands depends very much on the quality of the raw material, the growing conditions, the possible doping and on the time left between the end of the irradiation and the transmission measurement. The absorption coefficient derived from these measurements gives an evaluation of the density of the colour centres responsible for these absorption bands. Fig 13a and b shows the absorption coefficient as a function of the wavelength for 3 typical crystals, respectively 2 hours and 1 month after a 1000Gy irradiation. As already said, the crystal CF169 (undoped and grown from a purified raw material) does not suffer any damage. Another undoped crystal but grown from a poor quality raw material (CF30) shows some signs of damage immediately after irradiation with a very small improvement one month later. On the other hand a barium doped crystal (CF205) has a very strong damage in the first hours which recovers dramatically in time, up to the point where it is less damaged after one month than the undoped crystal. This very fast recovery can explain that the importance of the initial damage may have been underestimated and why the barium doping has been advertised to enhance the radiation resistance of CeF3 crystals [6]. In practice the importance of the initial damage and the rapid change in the optical performances could give severe problems for the control of the stability of a calorimeter at LHC, unless the recovery is actually much faster than the accumulated damage. A test is now on the way at a dose rate similar to the LHC to study the behaviour of barium doped crystals under realistic conditions.

It is now well established that the colour centres are related to impurities or defects in the crystal. This is confirmed by the very strong gradient of damage observed along the growth axis of some long crystals after a uniform irradiation perpendicular to this axis [10]. This gradient most probably reflects the segregation of impurities during the growth process. We have also observed some correlation between the displacement of the band edge and the amplitude of the initial damage. Oxygen contaminated crystals also show an increase of the damage. It is very likely that divalent cations (like barium) and oxygen in the O^{2-} form are impurities favouring the creation of fluorine vacancies which certainly play a dominant role in the formation of the observed colour centres.

For the crystals suffering radiation damage, a reduction of the light yield is observed simultaneously to the creation of the absorption bands. We have recorded the optical transmission and the light yield of a Ba doped crystal (CF205) for various damage levels up to a reduction by a factor 2 of the optical transmission at the wavelength of the peak emission

for the scintillation (340nm for this crystal). The correlation, with a slope about unity, is excellent as can be seen on Fig 14 and supports the idea that the radiation induced damage is mostly dominated by the absorption of colour centres. A direct evidence of the fact that the scintillation yield and spectrum are not modified by radiation was already given by the measurement of thin (absorption free) slices of CeF3 [10].

4.2 Damage as a function of the γ dose

Two undoped (CF30 and CF202) and one doped (CF204) crystals have been irradiated in Geneva in steps of about 250Gy up to 1230Gy. Another doped crystal (CF278) was irradiated at Brookhaven in seven steps up to an accumulated dose of 35kGy (3.5 Mrad). One undoped crystal of the intermediate category (see § 3.1 and 3.2) was irradiated at ENEA Rome, in 6 steps up to a total dose of 102kGy. Although the position of the absorption bands is the same for the undoped and doped crystals (340nm and 385nm for the most important one, plus a weak and broad band at 540nm), the kinetics of the formation of these bands as a function of the absorbed dose is dramatically different for the two sets of crystals. For the undoped crystals the damage quickly saturates at all wavelengths (250Gy for CF30 and 1000Gy for CF306) whereas for the doped crystals the saturation is not yet reached at 35kGy. The absorption coefficient at the peak of the absorption bands (340nm and 385nm) is plotted on Fig 15 and shows the rapid saturation for CF30 and CF306, although at a different dose and a very different damage level, probably to be related to a difference in the concentration of defects. The asymptotic behaviour for CF278 corresponding to a possible saturation at a much higher value of about 40kGy is clearly visible. It is to be noticed that for all the crystals the two absorption bands at 340nm and 385nm have a very similar behaviour with the increasing dose, suggesting that they are associated to the same colour centre.

4.3 Damage for low γ dose rate

One pure crystal (CF128) has been irradiated for two periods of about 100 days each at an average rate of 1.2Gy/hour, similar to the expected dose rate at LHC for $\eta = 2$ at about 4 m from the interaction region. The total accumulated dose was 5.3 $\pm$ 1.1kGy. At the end of each period a transmission measurement was made and compared to the transmission before irradiation. No damage was observed and all the transmission curves are within the measurement errors which corresponds to an attenuation length of at least 2 meters.

A similar test will be started soon with a Ba doped crystal in order to see whether or not the recovery is fast enough to compensate the damage induced at this dose rate.

4.4 Neutron induced damage

Two crystals (CF04 and CF05) have been irradiated by MeV neutrons in Bombay. The irradiation was done in 8 steps as described in table 4.

Irradiation time (days)	Duration (mn)	Fluence of MeV neutron (cm^{-2})	Integrated fluence (cm^{-2})
0	17	1×10^{11} cm^{-2}	1×10^{11} cm^{-2}
2	33	2×10^{11} cm^{-2}	3×10^{11} cm^{-2}
4	66	4×10^{11} cm^{-2}	7×10^{11} cm^{-2}
16	165	1×10^{12} cm^{-2}	1.7×10^{12} cm^{-2}
49	331	2×10^{12} cm^{-2}	3.7×10^{12} cm^{-2}
57	825	5×10^{12} cm^{-2}	8.7×10^{12} cm^{-2}
64	825	5×10^{12} cm^{-2}	1.4×10^{13} cm^{-2}
67	825	5×10^{12} cm^{-2}	1.9×10^{13} cm^{-2}

Table 4 : Neutron irradiation conditions

The variation of the optical transmission at 4 different wavelengths (320nm, 360nm, 400nm and 440nm) is plotted in Fig 16a and 16b for the 2 crystals as a function of the integrated neutron fluence. The first crystal (CF04) does not show any appreciable loss of transmission up to an irradiation of about $10^{12}cm^{-2}$. However, at higher neutron fluence, the transmission drops from 80% to about 60% in the UV region ($\lambda \leq 400nm$). This crystal shows a similar drop in transmission after a gamma irradiation of 100Gy which is the residual gamma flux expected in the irradiation chamber after the lead shield. On the other hand, the crystal CF05 which is more radiation hard to gamma rays, does not show any transmission loss over the entire wavelength range explored (290nm to 900nm) up to the maximum integrated neutron fluence (1.9×10^{13} cm^{-2}). We can therefore conclude that cerium fluoride crystals, even of rather poor quality (CF04), are not damaged by fast neutrons, at least up to a fluence of a few $10^{13}cm^{-2}$.

The crystals did not develop significant amount of radioactivity. The γ activity was always at the background level (0.1 mr/hour). The β activity has been measured to be 0.07 mr/hour after an irradiation of $5x10^{12}cm^{-2}$ MeV neutrons, dying out with a typical lifetime of 12 hours.

4.5 Recovery at room temperature

As already discussed, a spontaneous and fast recovery at room temperature was observed for the barium doped crystals at the different places where irradiation tests were made (Brookhaven, CERN and ENEA). This is illustrated for the crystal CF278 on Fig 17 where the absorption coefficient (proportional to the density of colour centres) corresponding to the 3 absorption bands at 340nm, 385nm and 540nm is plotted as a

function of time after a 10kGy irradiation. Most of the damage has disappeared after about 2 days. For some other doped crystals (CF204 and CF205) a residual and stable damage remains one month after the fast initial recovery. It is interesting to notice that within the precision of the measurements the kinetic of annealing is exactly the same for the 2 UV absorption bands at 340nm and 385nm, whereas the 540nm band recovers faster, at least in the first hours. Reirradiating the crystal CF278 after 60 hours of recovery from the total dose of 35kGy with an additional 1000Gy shows that most of the initial damage reappears quickly, followed by a recovery which is just as fast as after the initial irradiation.

We have applied the same procedure for two undoped crystals suffering radiation damage (CF30 and CF202) after an irradiation of 1000Gy, for which the damage saturation was already reached (see § 4.3). The 2 UV absorption bands have again a similar behaviour, but very different from the doped crystals (Fig 17). There is only a small recovery in the first hour and then the crystal remains damaged and stable for a very long time (measurements over more than 3 months). One can assume that this residual damage level depends very much on the quality of the raw material and on the growth process: it is actually different for CF30 and CF202 and some undoped crystals have no damage at all. In the example shown on Fig 17 the barium doped crystal becomes less damaged after about 12 hours than CF30. This can easily explain why barium doping seems to have a positive effect on the radiation hardness for crystals grown from poor quality raw material, particularly if the measurements are not done immediately after the irradiation.

4.6 Thermal bleaching

After the initial damage recovery at room temperature we have applied a thermal treatment on those crystals which have a residual damage several weeks after the irradiation. This concerns the undoped crystals (CF30 and CF202) as well as some of the barium doped crystals (CF204 and CF205) for which the room temperature recovery is not complete. The crystal CF207 belonging to the intermediate category as defined in § 3.2 was also tested in the same way. The crystals were heated at increasing temperatures up to 900°C in several steps of about 50°C in a vacuum furnace (10^{-5} torr) for six hours. After each step they were measured in transmission immediately after cooling.

A very small recovery can be seen after a thermal cycle at 150°C for the barium doped crystal (CF204) as well as for CF207. The annealing is complete for a temperature of 300°C (Fig 18a). For the undoped crystals the situation is different. A sizeable recovery is already observed at 150°C. On the other hand a residual damage is observed after the thermal cycle at 300°C (Fig 18b). More detailed study between 150°C and 300°C is on the way. For all the crystals the rate of recovery of the 2 absorption bands is exactly the same.

When the crystals are heated at temperatures exceeding 300°C the absorption band at 385nm is further annealed in the case of an incomplete recovery at 300°C. On the other hand, for all the crystals, a single absorption band is produced at 340nm and increases rapidly with the temperature. A slight shift from 340nm to 320nm is observed when the temperature is raised from 300°C to 900°C (Fig 19). In fact a black deposit is clearly visible on the surface of the crystal and this thermally induced damage seems to be located in the first 1 or 2 mm from the surface. A similar annealing procedure is applied to all crystals just after the growth without producing such effects, the only difference being that the crystal stays under vacuum all the time between the growth and the annealing process. It is well known that fluorine vacancies are easily produced near the surface of fluorine crystals. Under normal atmosphere oxygen atoms can diffuse in the crystal to compensate the charge imbalance. At high temperature, precipitates of cerium oxyfluoride can be created which are responsible for the black deposit and for the absorption band at 340nm. If the raw material is not sufficiently oxygen free or if the vacuum conditions of the furnaces are not good enough a similar effect can be produced in the bulk of the crystal during the growth. This is in practice one of the most frequent causes of bad quality crystals.

4.7 Optical bleaching

Similarly to the thermal bleaching we have tried to anneal the residual damage observed in some crystals by means of exposure to light. A 50mW argon laser (514nm) did not produce any effect even after several hours. UV lamps (mercury and xenon) were then tested and the best results were obtained with the light of a 150W xenon lamp collimated on the crystal. The light source was filtered at 300nm to limit the creation of free carriers by exciting the crystal at a too high energy.

The evolution of the absorption coefficient for the 2 bands at 340nm and 385nm is plotted on Fig 20 for crystal CF205 as a function of the exposure time to the xenon light. The behaviour is rather complex and cannot be fitted by one or two exponentials. A fast recovery in the first 2 hours is followed by a much slower one, which seems to saturate before total bleaching is reached. Once again the evolution of the 2 bands is exactly the same.

4.8 Thermoluminescence

For most of the crystals the thermoluminescence signal is either non-existent or very weak for the residual damage. For the initial damage of the barium doped crystals several glow peaks could be observed with an intensity of about 2 orders of magnitude less than what is observed in BaF2. The data show 2 prominent peaks at about 140°C and 250°C with a small peak in between (Fig 21). Further studies to determine the kinetics of these peaks and to correlate them with the recovery in optical transmission are on the way.

4.9 Discussion on radiation damage

In all cases the similarity of the behaviour of the 2 absorption bands at 340nm and 385nm is evident. The saturation as a function of the dose, the recovery at room temperature, the thermal and optical bleaching are exactly the same for these 2 bands for all the crystals which are not 100% radiation hard. This similarity strongly suggests that these bands are associated to the same colour centre in 2 different configurations. Polarization studies of the absorption bands show that the damage is highly polarized by the crystal field which supports the idea that the colour centre is a trap for an electrical carrier, electron or hole. More precisely, the relative amplitude of the 2 absorption bands strongly depends on the polarization of the incident light (Fig 22) which again suggests 2 different sites. The most probable defect in cerium fluoride crystals is a fluorine vacancy which can trap an electron (F centre). In the tysonite structure (CeF3, LaF3, PrF3) there are 2 types of fluoride sites with different cerium coordination. Therefore 2 types of F centers can be produced with slightly different electronic configuration and optical properties, but the same kinetics for formation and annealing. It is very likely that the F centres play a dominant role in the damage of CeF3, either directly or through their participation in the formation of more complex colour centres, involving oxygen or cationic impurities.

5. Conclusions:

The optical properties and the radiation damage behaviour of 22 cerium fluoride crystals (some of them Ba doped) grown by 5 different producers have been studied. The optical transmission of all the crystals is in general good and close to the theoretical value with a sharp band edge and no visible absorption band. Although there is some dispersion of the results depending on the crystal quality and the conditions of the growth, the crystals can be classified in 2 categories depending on whether or not they are doped. These categories can be easily identified by the position of the band edge which is slightly red-shifted for the doped crystals.

The light emission of the undoped crystals has 2 fast components (about 10nsec and 30nsec) and shows some signs of diffusion of excitation to cerium ions in perturbed sites. For a large number of crystals the emission spectrum has one peak at 300nm and a smaller and broader one at 340nm. The luminescence spectrum of the doped crystals is more complex and extends to longer wavelengths. The decay time is about 30nsec but the 10nsec component is not visible anymore. The light yield of all the crystals is directly correlated to the position of the band edge, which gives a reduction of nearly 50% for the barium doped crystals. After a continuous improvement in the production process the light yield for undoped crystals has reached about 1500 photons/MeV.

When exposed to a few kGy of γ rays some of the good quality crystals do not show any damage at low and high dose rate. Crystals grown from poor quality raw material or barium doped crystals suffer a light yield

reduction associated to the creation of 2 strong absorption bands at 340nm and 385nm and in some cases a weaker one at 540nm. For a second class of undoped crystals of "reasonable" quality, the damage is moderate and saturates already at 250Gy. On the other hand it is very stable at room temperature and recovers only partially at 300°C. The initial damage of the doped crystals is much higher and saturates at much higher doses (40kGy). On the other hand it recovers very fast at room temperature and the residual damage (when it exists) was fully annealed between 150°C and 300°C. Optical annealing, although less efficient than for BGO or BaF2 can help recovering a good fraction of the residual damage.

From all our measurements described in this report it seems preferable to use undoped crystals for applications in severe environment like LHC, because of their higher light yield, the possibility to be perfectly radiation hard up to at least a few kGy or in the worst case to have a rapidly saturating damage which is then stable in time. Several samples of regularly increasing length already meet the performances needed for use at LHC. A better understanding of the required purity level and control should allow the producers to grow long crystals of the same quality in a relatively short future.

6. Acknowledgements:

The authors wish to express their gratitude to the teams of the companies Monkrystaly Turnov (Czech Republic), NKK (Japan), Optovac (USA), Shanghaï Institute of Ceramics (China) and Vavilov State Optics Institute (Russia) for the procurement of crystals and their flexibility in changing the production parameters to fit our requirements. We are indebted to Dr. V. Reiterov from the Petersburg State Optical Institute and particularly to Dr. R. Sparrow from Optovac for a continuous exchange of information and very constructive discussions. We would like also to thank the technicians of the different radiation facilities we have used at the Hospital Cantonal in Geneva (Switzerland), the Apsara reactor in Bombay (India), the Brookhaven National Laboratory (USA), the Calliope facility at ENEA, Rome (Italy), and Saclay (France). The help from several technical services at CERN for cutting, polishing and annealing the crystals was also highly appreciated.

References:

[1] P. Lecoq et al, Homogeneous calorimeters at LHC/SSC, Second International Conference on Calorimetry in High Energy Physics, World Scientific p283 (1992)
CERN Preprint 91- 231

[2] W.W. Moses and S. E. Derenzo, IEEE Trans. Nucl. Sci. NS-36 (1989) 137

[3] D.F. Anderson, IEEE Trans. Nucl. Sci. NS-36 (1989) 137
and NIM A287 (1990) 606

[4] R&D Proposal for the study of new fast and radiation hard scintillators for calorimetry at LHC
Crystal Clear Collaboration , CERN / DRDC P27 / 91-15, project RD-18

[5] R. Sparrow, private communication

[6] A.A. Asseev et al, Proceedings of the Second International Conference on Calorimetry in High Energy Physics, Capri, October 1991, World Scientific p313 (1992)

[7] L.M. Bollinger and G.E. Thomas, Rev. Sci. Instr. 32 (1961) 1044

[8] G. Hass, J.B. Ramsey, R. Thun, J. Opt. Soc. Am. Vol 49, No2 (1959) 116

[9] C. Pedrini et al, J. of Phys. Cond. Matter, 4,5461 (1992)

[10] P. Lecoq, CERN-PPE Preprint 92-205, Proceedings of IEEE Nuclear Science Symposium, Orlando, October 27-31, 1992.

Figure caption:

Fig 1: Optical transmission spectra for 2 undoped crystals grown with the same process for 2 different qualities of the raw material:
CF30: 200 ppm Nd^{3+} contamination, CF128: ≤ 2ppm Nd^{3+}

Fig 2: Transversal optical transmission spectra (thickness 20 mm) measured in different distances from the seed along the growth axis of a poor quality crystal (CF171 undoped)

Fig 3: Transmission band edge for several crystals

Fig 4: Optical transmission and photo-luminescence spectra for different excitation wavelengths of crystals: a- CF169 undoped, purified
b- CF202 undoped
c- CF205 barium doped

Fig 5: Anticorrelation between the amplitudes of the 2 emission bands at 286nm and 340nm for undoped crystal (CF130) at different excitation wavelengths

Fig 6: Optical transmission and radio-luminescence spectra with a Cs^{137} source for one undoped (CF130) and one barium doped crystal (CF205)

Fig 7: Low temperature excitation spectra for
a- a weakly cerium doped (0.05%) lanthanum fluoride crystal
b- a 100% cerium doped lanthanum fluoride crystal (pure CeF3)

Fig 8: Decay time curves for crystals: a- CF130 undoped
b- CF205 barium doped

Fig 9: Decay time curves at several emission wavelengths for crystals:
a- CF130 undoped
b- CF205 barium doped

Fig 10: Light yield as a function of the integrating gate for undoped crystal (CF169)

Fig 11: Correlation of the light yield and the band edge wavelength for several crystals

Fig 12: Optical transmission spectra of crystal CF128 (thickness 18 mm, undoped) as a function of the Co^{60} dose

Fig 13: Absorption coefficients of 2 undoped crystals (CF169 and CF30) and one barium doped crystal (CF205) a- 2 hours and b- one month after a 1000Gy Co^{60} irradiation

Fig 14: Correlation of the optical transmission and the light yield of barium doped crystal (CF205) at different steps of radiation damage

Fig 15: Absorption coefficient at the peak of the 2 most important absorption bands (340nm and 385nm) as a function of the Co^{60} dose for two undoped crystals (CF30 and CF306) and one barium doped crystal (CF278)

Fig 16: Optical transmission loss at 4 different wavelengths for undoped crystals (CF04 and CF05, thickness 10 mm) as a function of the neutron fluence

Fig 17: Spontaneous recovery of the main absorption bands for one undoped (CF30) and one barium doped crystal (CF278)

Fig 18: Thermal annealing of crystals: a- CF204, barium doped
b- CF202, undoped

Fig 19: Thermal damage above 300°C for undoped crystal (CF207)

Fig 20: Optical bleaching for the 2 main absorption bands of barium doped crystal (CF205) as a function of the exposure time to a 150W xenon lamp

Fig 21: Thermoluminescence spectrum of barium doped crystal (CF278)

Fig 22: Optical transmission spectra of undoped crystal (CF30) after a 1000Gy Co^{60} exposure for 2 perpendicular directions of the polarization of the spectrophotometer beam

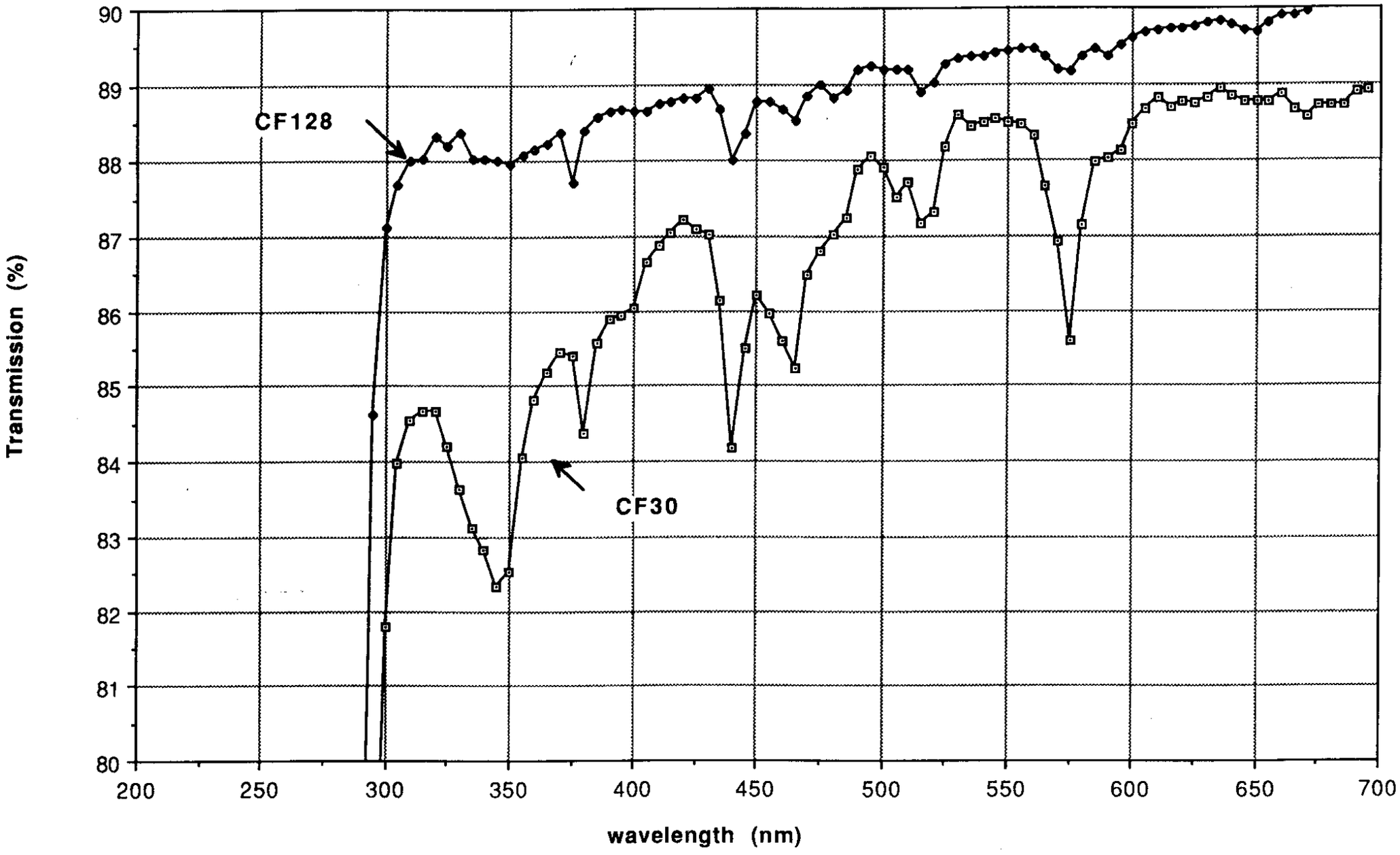
Transmission (%)
90
89
88
87
86
85
84
83
82
81
80
CF128
CF30
200
250
300
350
400
450
500
550
600
650
700
wavelength (nm)

Fig 1

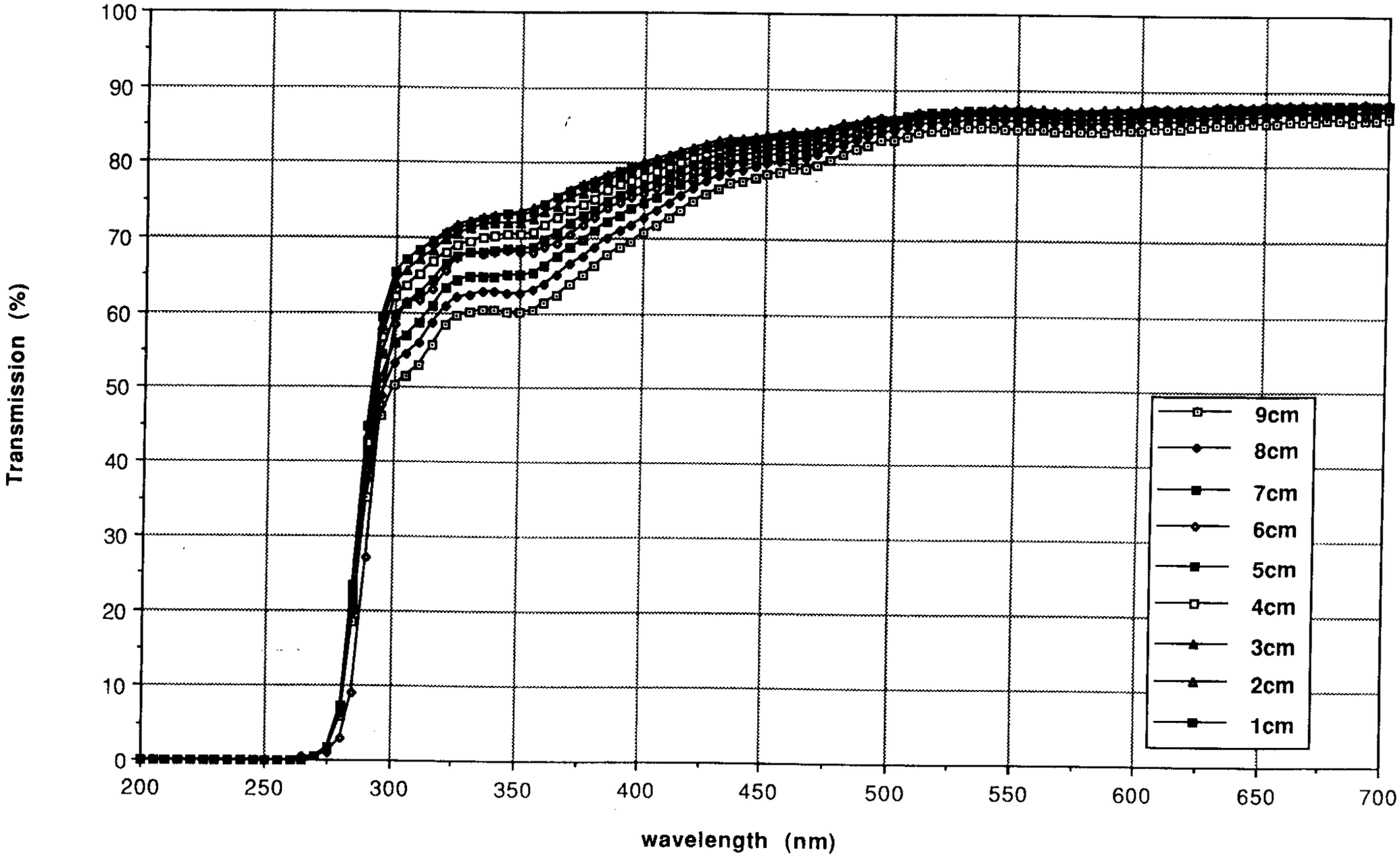
Transmission (%)
100
90
80
70
60
50
40
30
20
10
0
200
250
300
350
400
450
500
550
600
650
700
wavelength (nm)
9cm
8cm
7cm
6cm
5cm
4cm
3cm
2cm
1cm

Fig 2

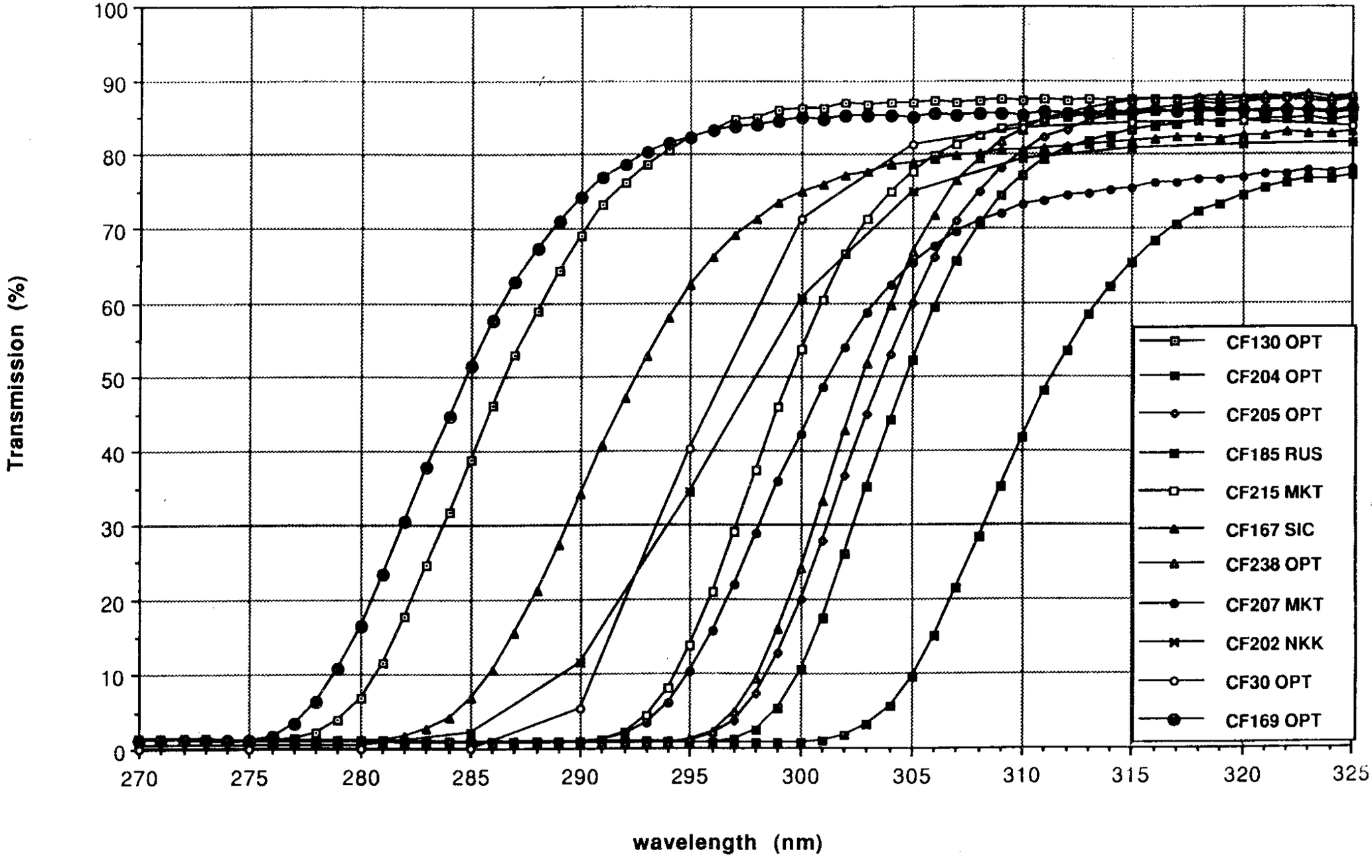
Transmission (%)
100
90
80
70
60
50
40
30
20
10
0
270
275
280
285
290
295
300
305
310
315
320
325
wavelength (nm)
CF130 OPT
CF204 OPT
CF205 OPT
CF185 RUS
CF215 MKT
CF167 SIC
CF238 OPT
CF207 MKT
CF202 NKK
CF30 OPT
CF169 OPT

Fig 3

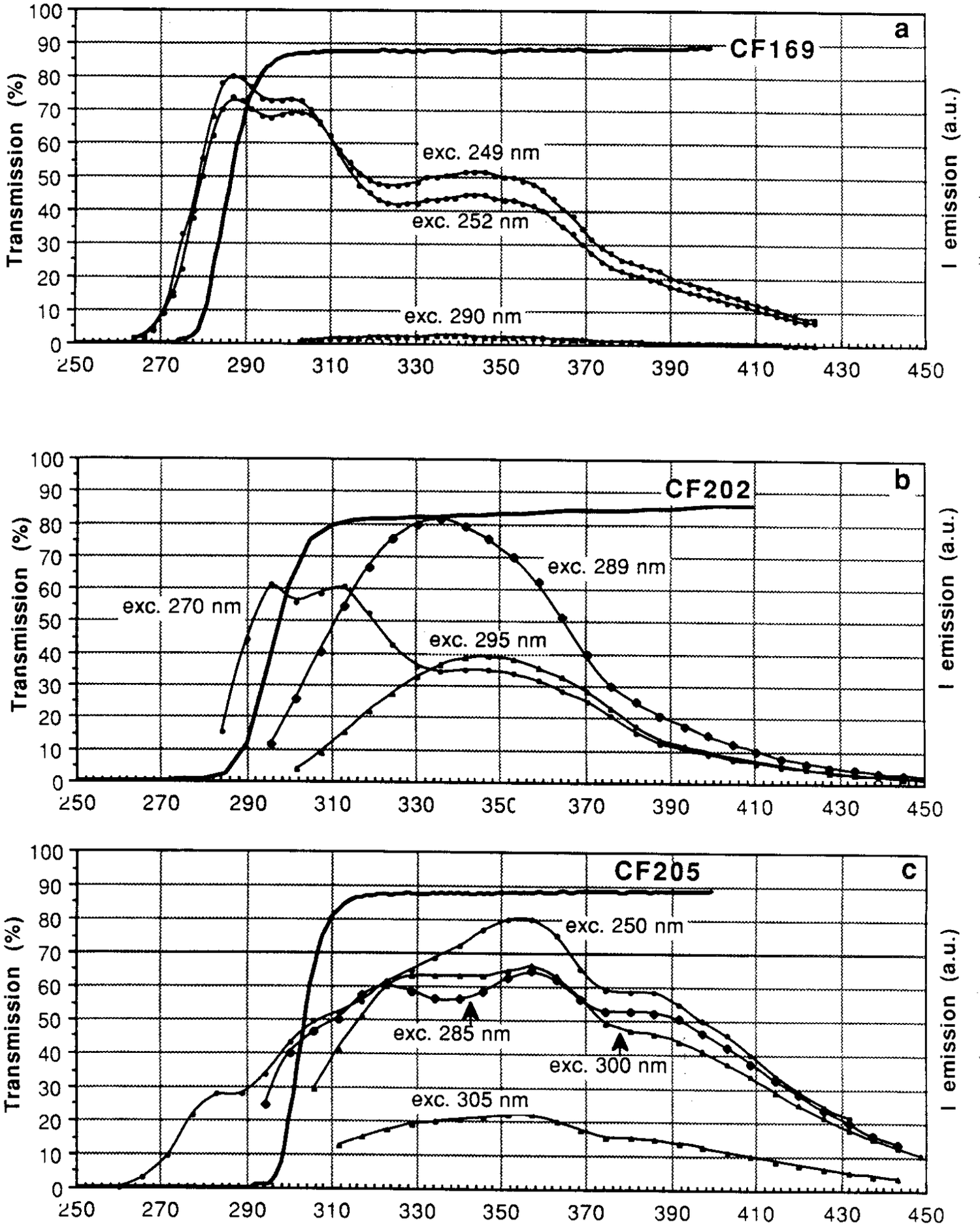
a
CF169
exc. 249 nm
exc. 252 nm
exc. 290 nm
b
CF202
exc. 289 nm
exc. 270 nm
exc. 295 nm
c
CF205
exc. 250 nm
exc. 285 nm
exc. 300 nm
exc. 305 nm
Transmission (%)
I emission (a.u.)
100
90
80
70
60
50
40
30
20
10
0
250
270
290
310
330
350
370
390
410
430
450

Fig 4

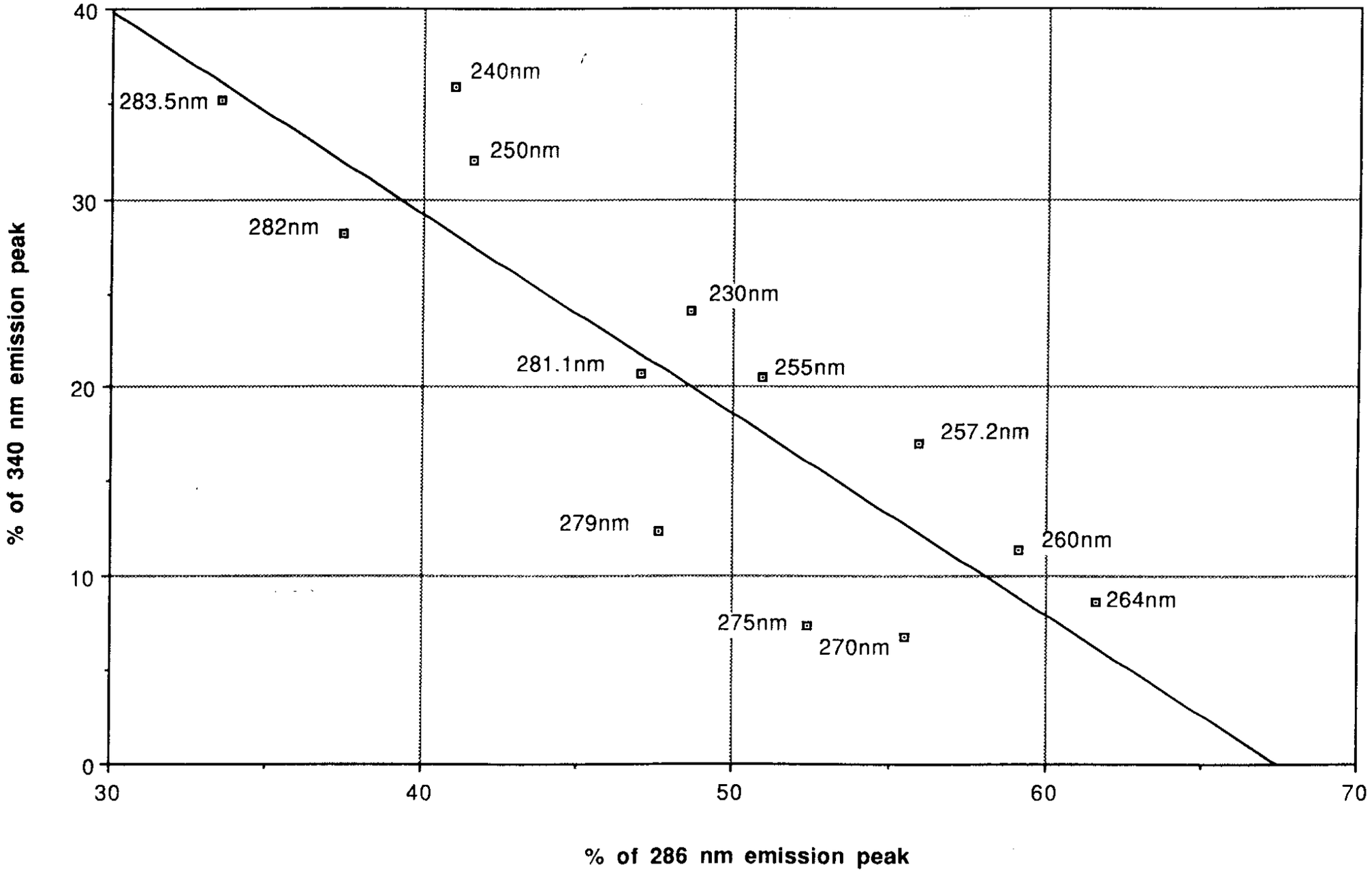
40
30
20
10
0
30
40
50
60
70
% of 340 nm emission peak
% of 286 nm emission peak
283.5nm
240nm
250nm
282nm
230nm
281.1nm
255nm
257.2nm
279nm
260nm
264nm
275nm
270nm

Fig 5

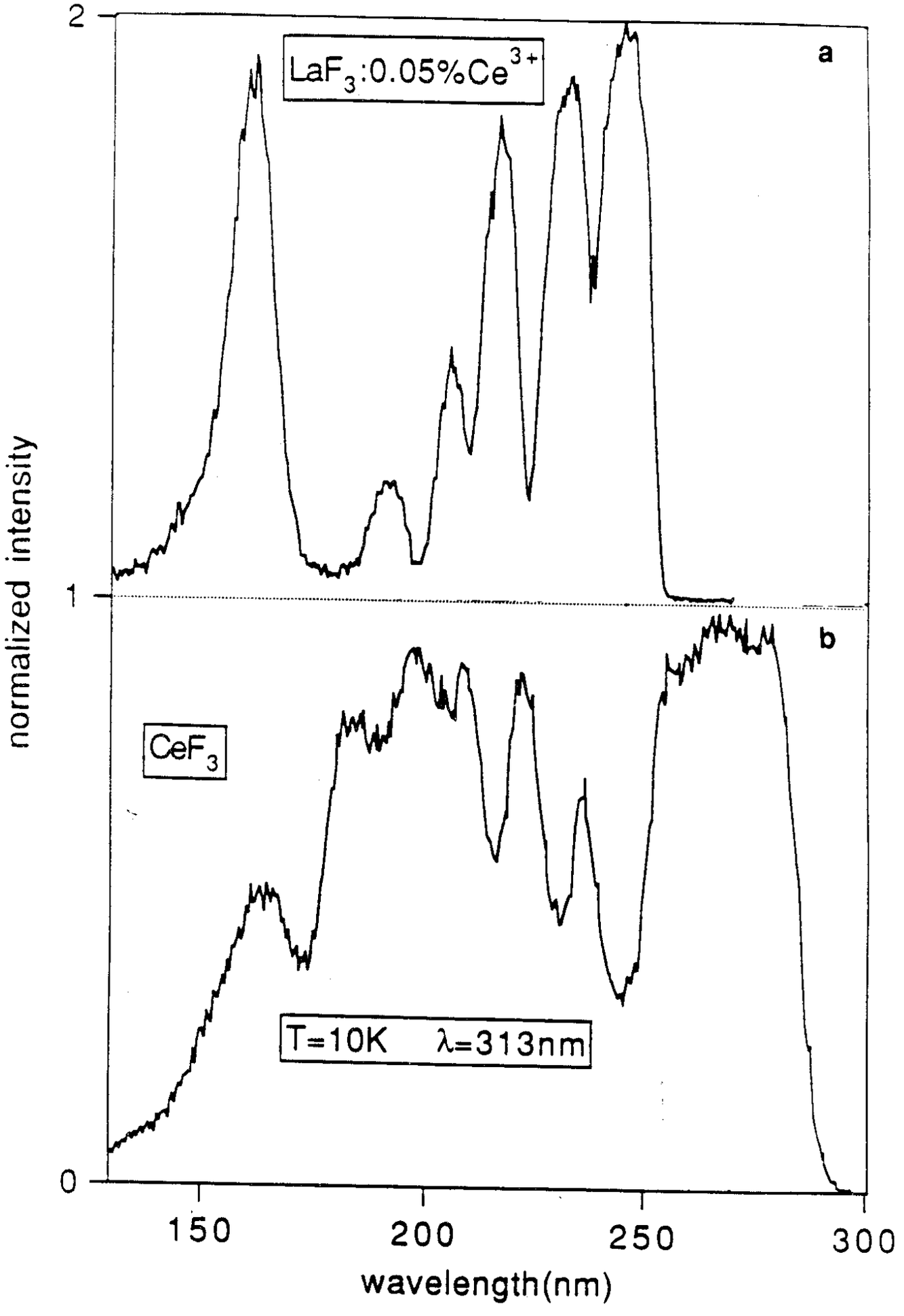
2
1
0
normalized intensity
LaF3:0.05%Ce3+
a
b
CeF3
T=10K λ=313nm
150
200
250
300
wavelength(nm)

Fig 7

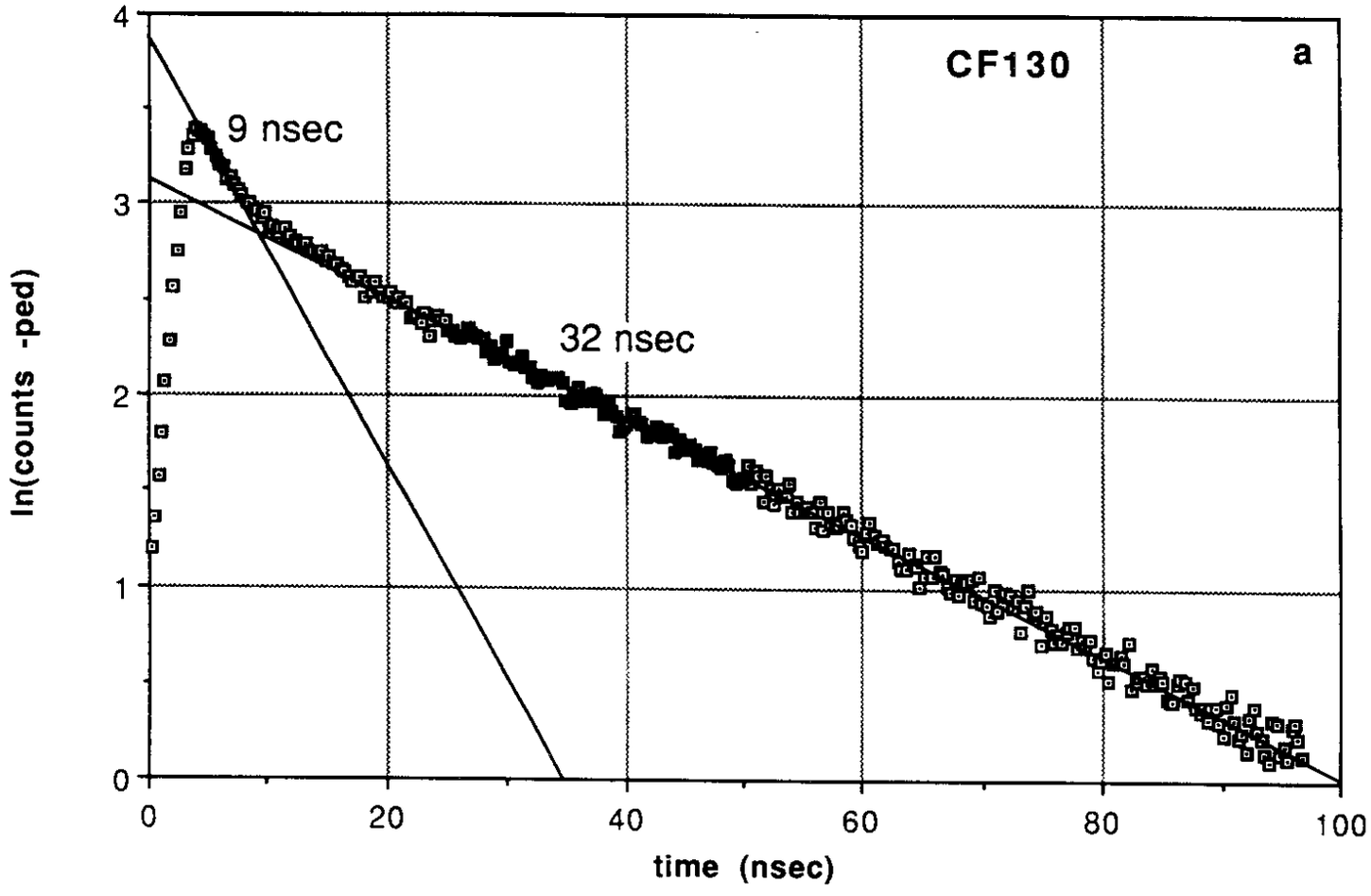
CF130
a
9 nsec
32 nsec
ln(counts -ped)
time (nsec)
0
1
2
3
4
0
20
40
60
80
100

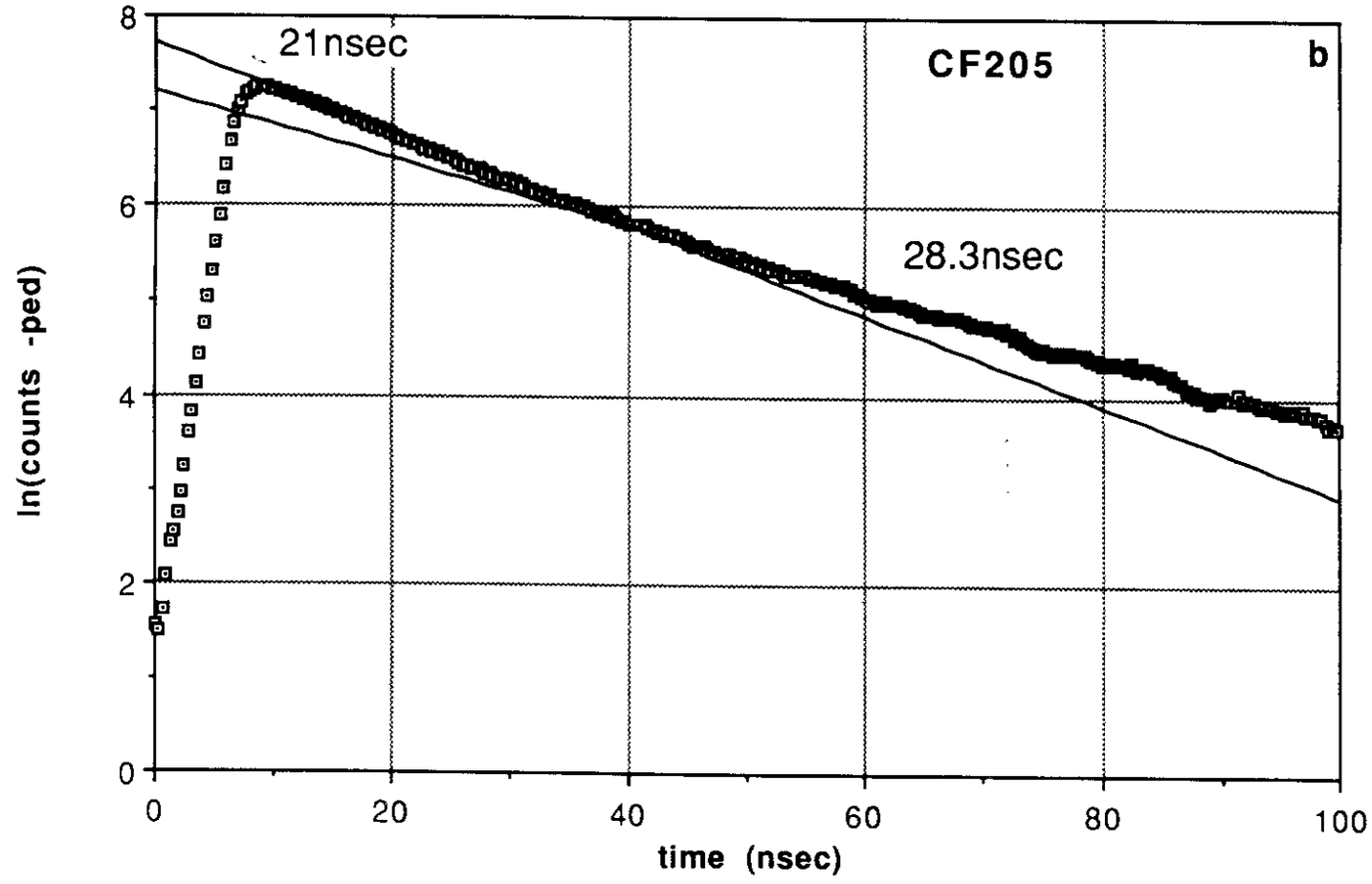
CF205
b
21nsec
28.3nsec
ln(counts -ped)
time (nsec)
0
2
4
6
8
0
20
40
60
80
100

Fig 8

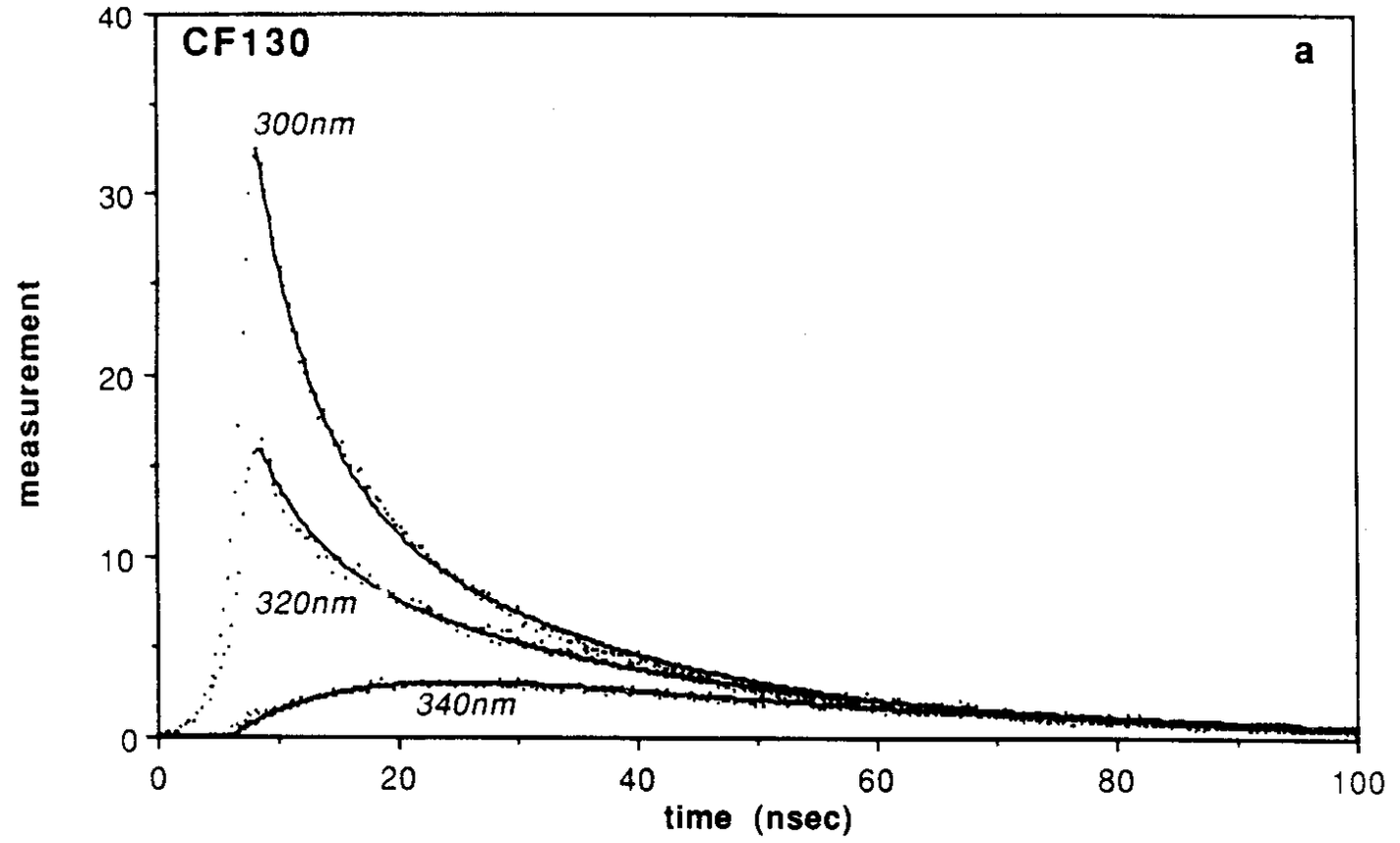
CF130
a
300nm
320nm
340nm
measurement
time (nsec)
0
10
20
30
40
0
20
40
60
80
100

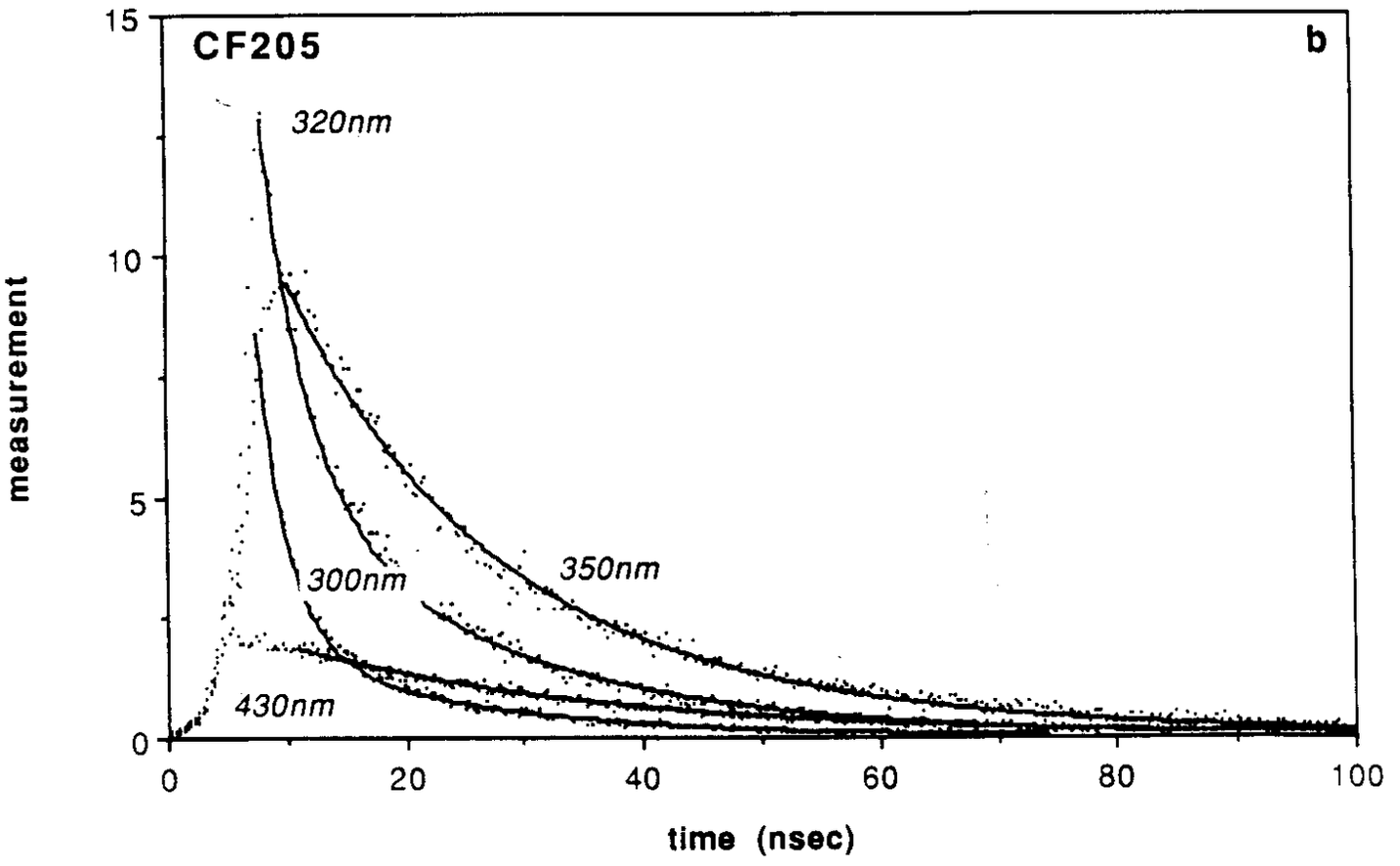
CF205
b
320nm
300nm
350nm
430nm
measurement
time (nsec)
0
5
10
15
0
20
40
60
80
100

Fig 9

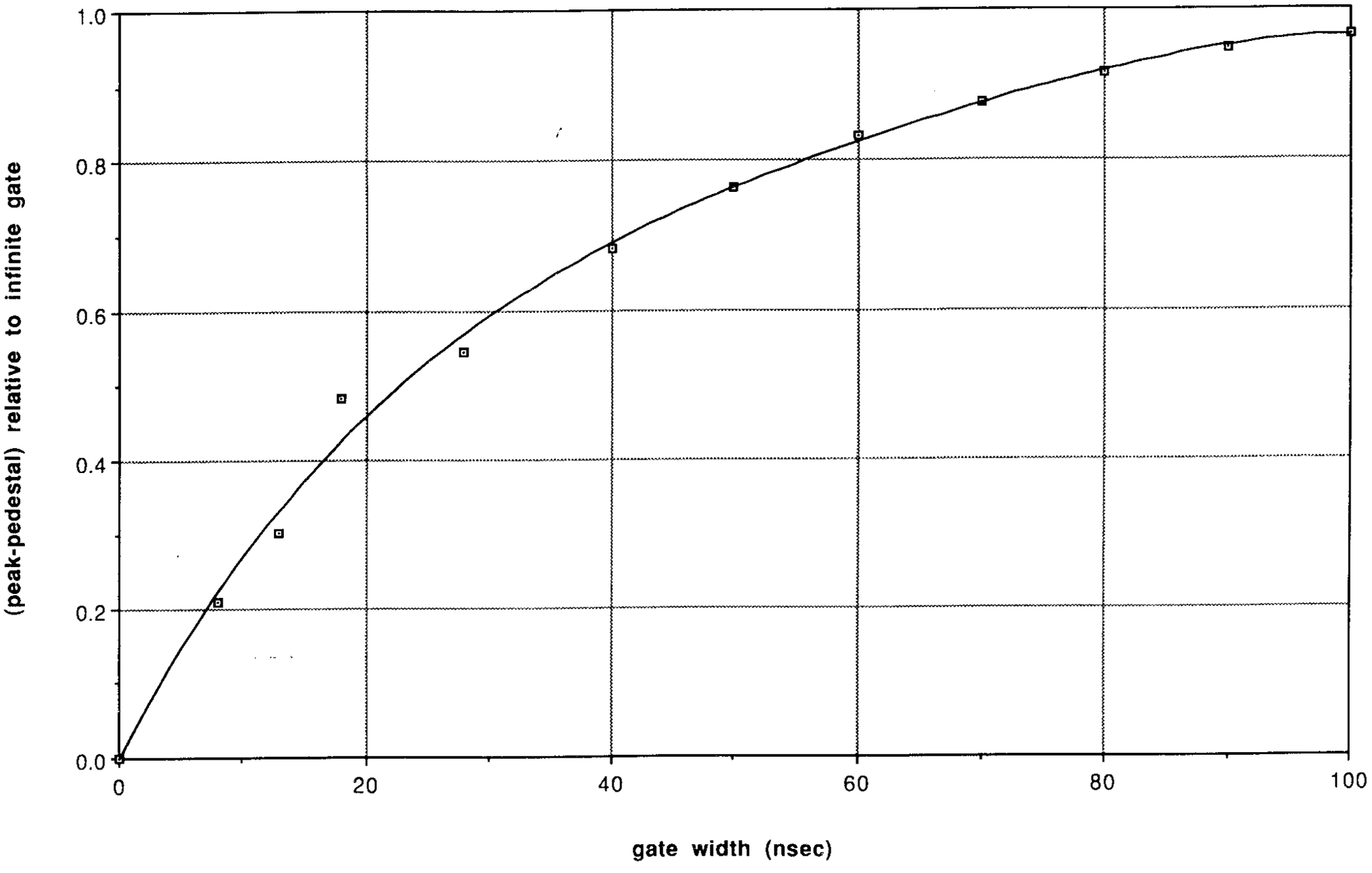
1.0
0.8
0.6
0.4
0.2
0.0
0
20
40
60
80
100
(peak-pedestal) relative to infinite gate
gate width (nsec)

Fig 10

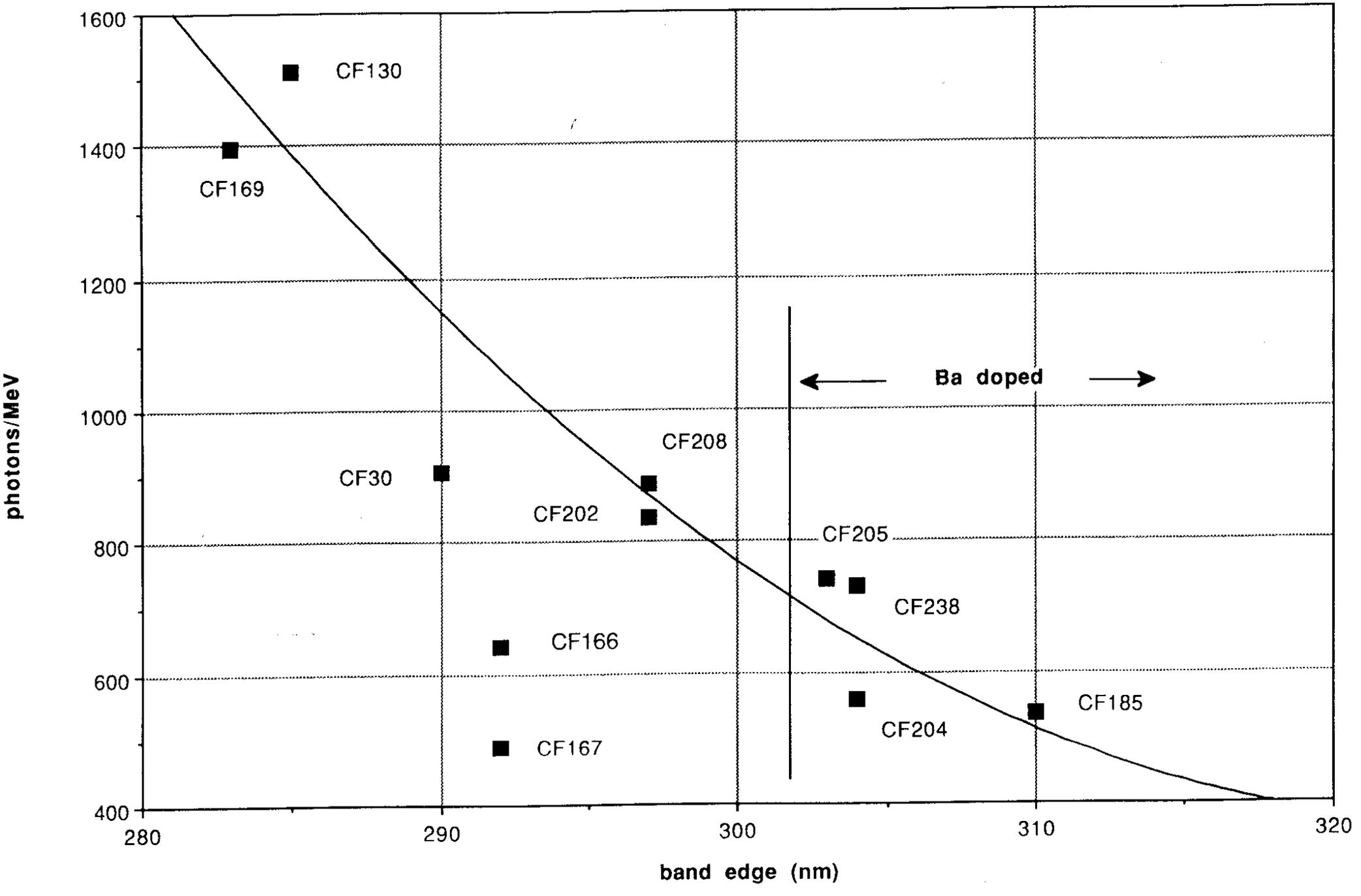
1600
1400
1200
1000
800
600
400
280
290
300
310
320
photons/MeV
band edge (nm)
CF130
CF169
CF30
CF208
CF202
CF205
CF238
CF166
CF167
CF204
CF185
Ba doped

Fig 11

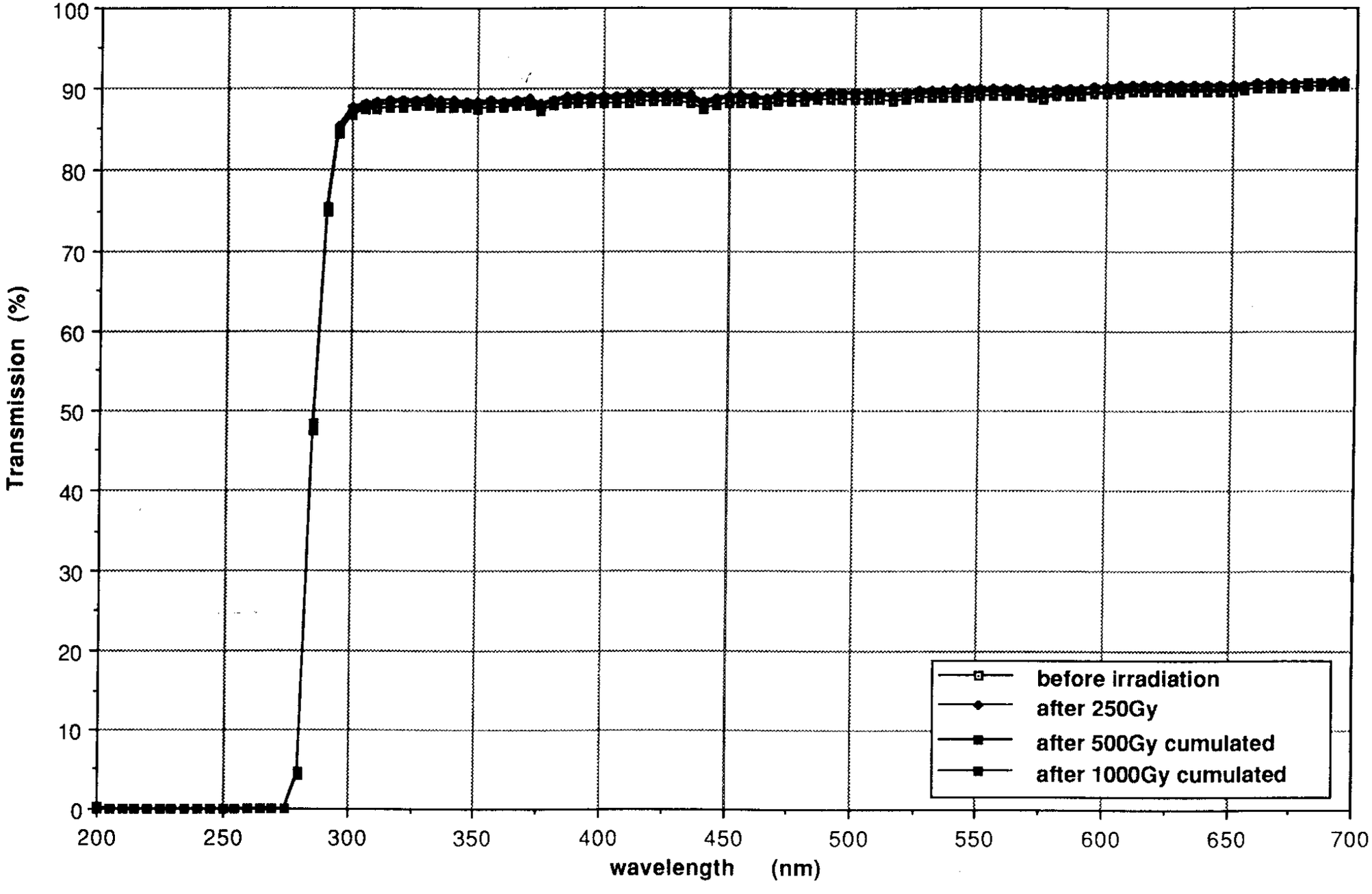
Transmission (%)
100
90
80
70
60
50
40
30
20
10
0
200
250
300
350
400
450
500
550
600
650
700
wavelength (nm)
before irradiation
after 250Gy
after 500Gy cumulated
after 1000Gy cumulated

Fig 12

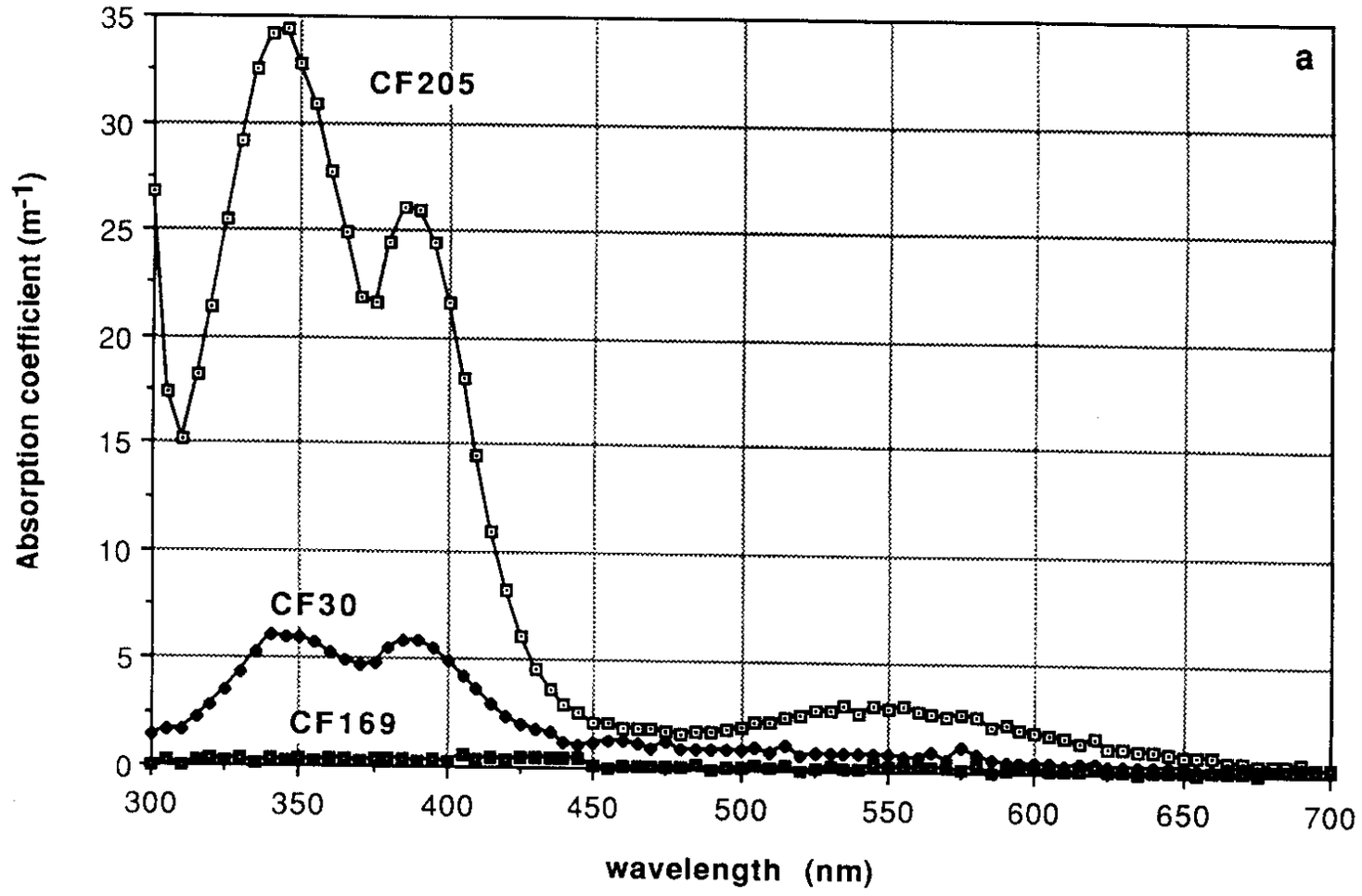
a
CF205
CF30
CF169
Absorption coefficient (m-1)
wavelength (nm)
0
5
10
15
20
25
30
35
300
350
400
450
500
550
600
650
700

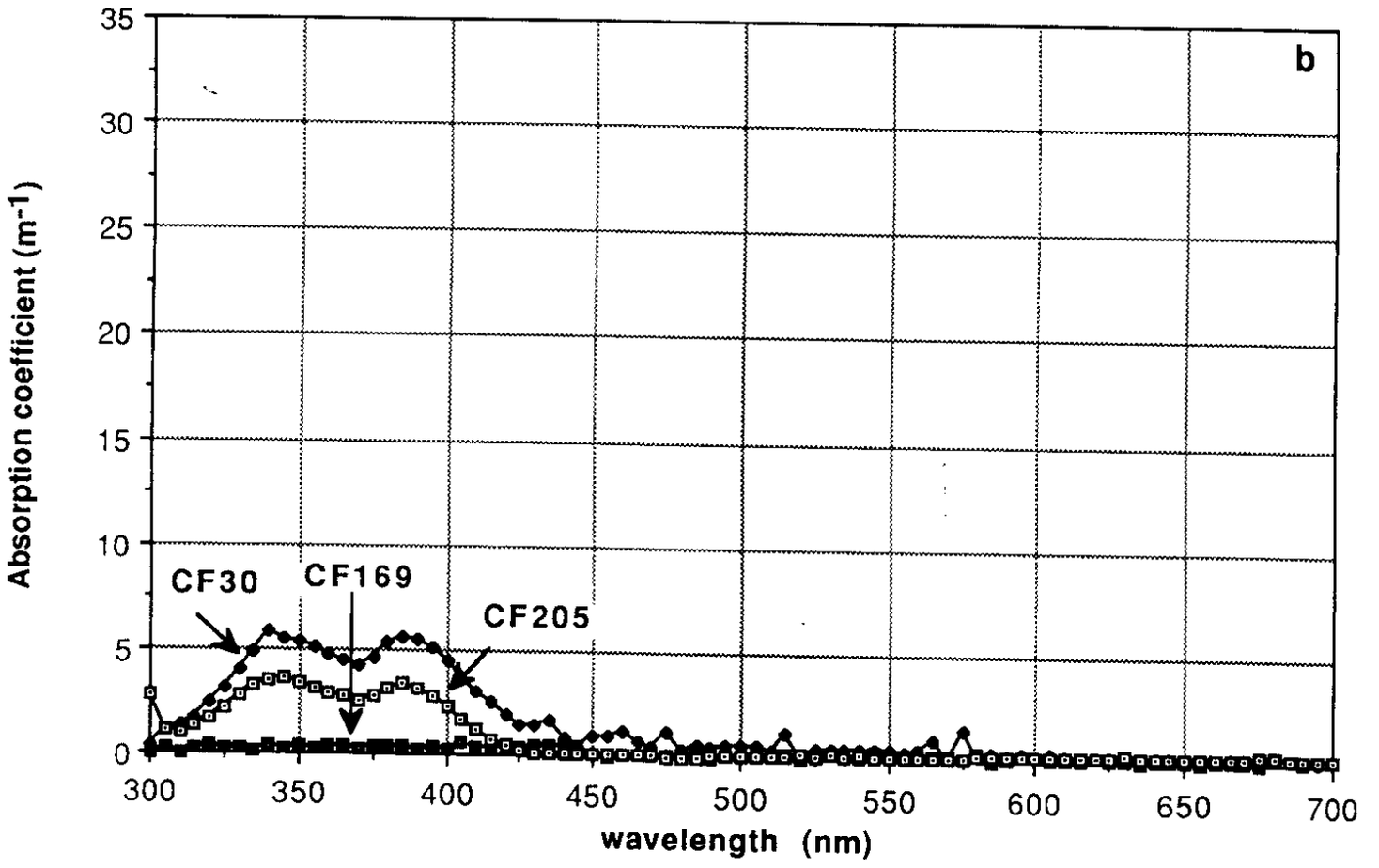
b
CF30
CF169
CF205
Absorption coefficient (m-1)
wavelength (nm)
0
5
10
15
20
25
30
35
300
350
400
450
500
550
600
650
700

Fig 13

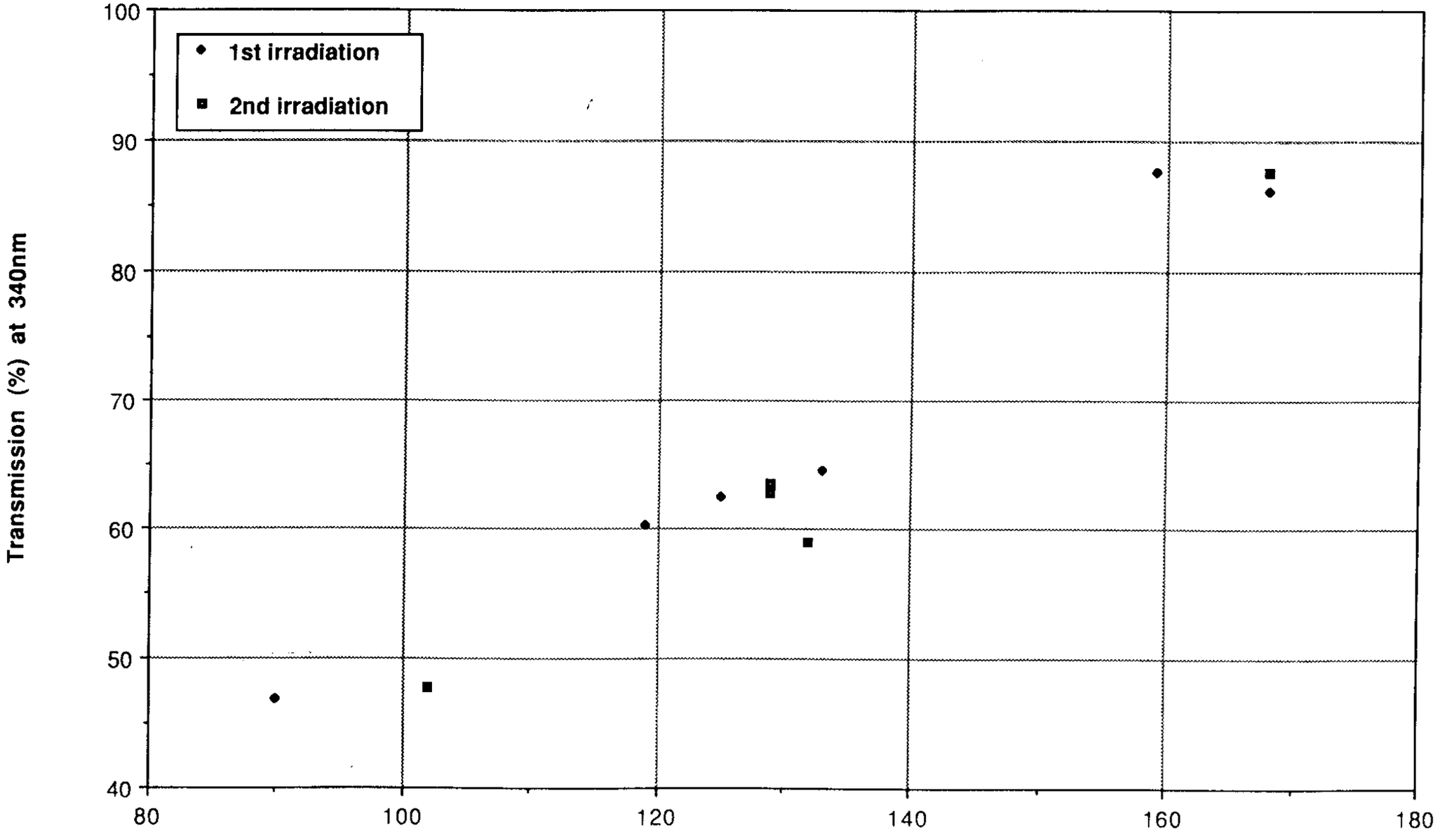
1st irradiation
2nd irradiation
Transmission (%) at 340nm
100
90
80
70
60
50
40
80
100
120
140
160
180
Photoelectrons/MeV

Fig 14

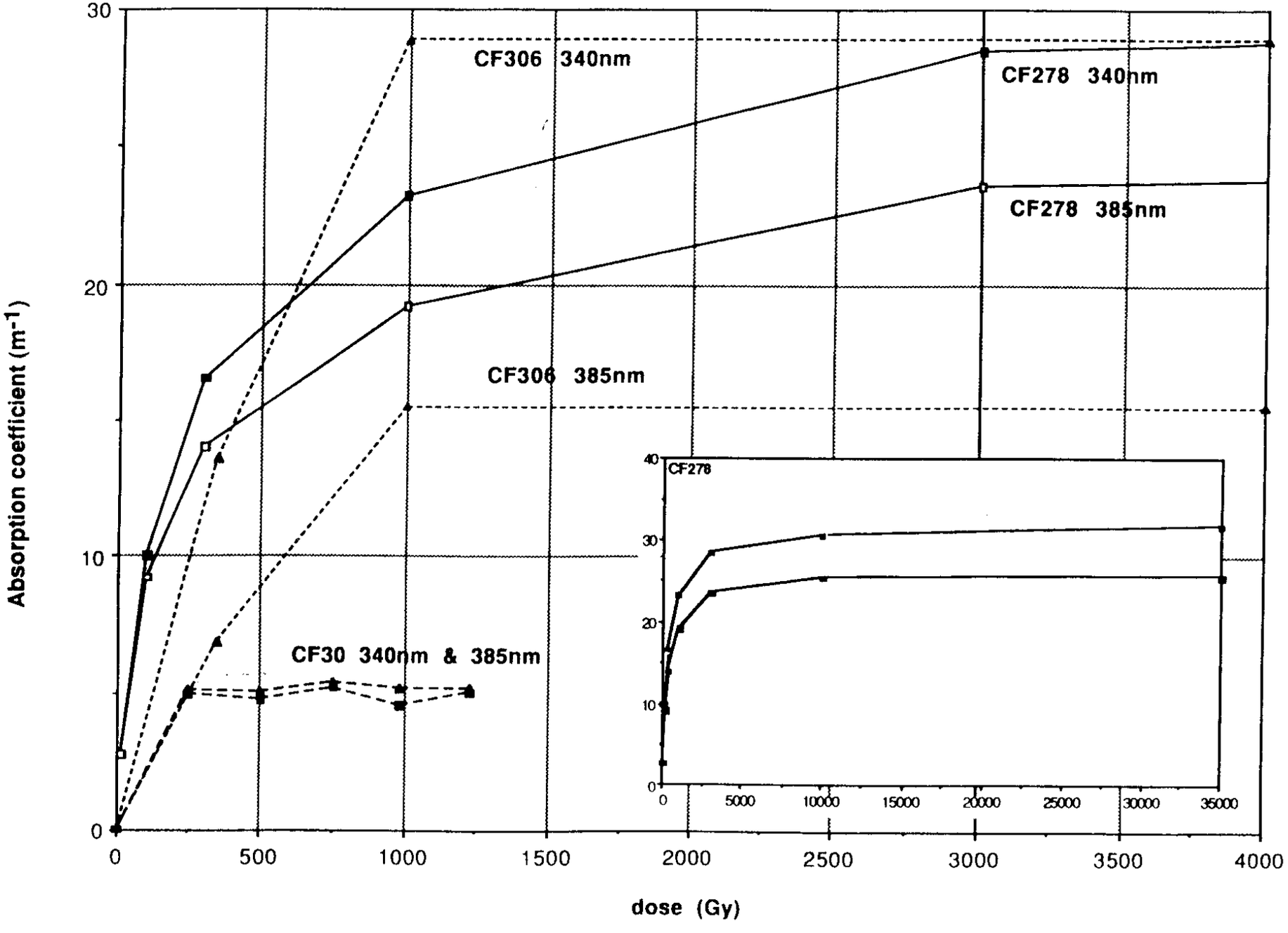
Absorption coefficient (m-1)
30
20
10
0
0
500
1000
1500
2000
2500
3000
3500
4000
dose (Gy)
CF306 340nm
CF278 340nm
CF278 385nm
CF306 385nm
CF30 340nm & 385nm
CF278
40
30
20
10
0
0
5000
10000
15000
20000
25000
30000
35000

Fig 15

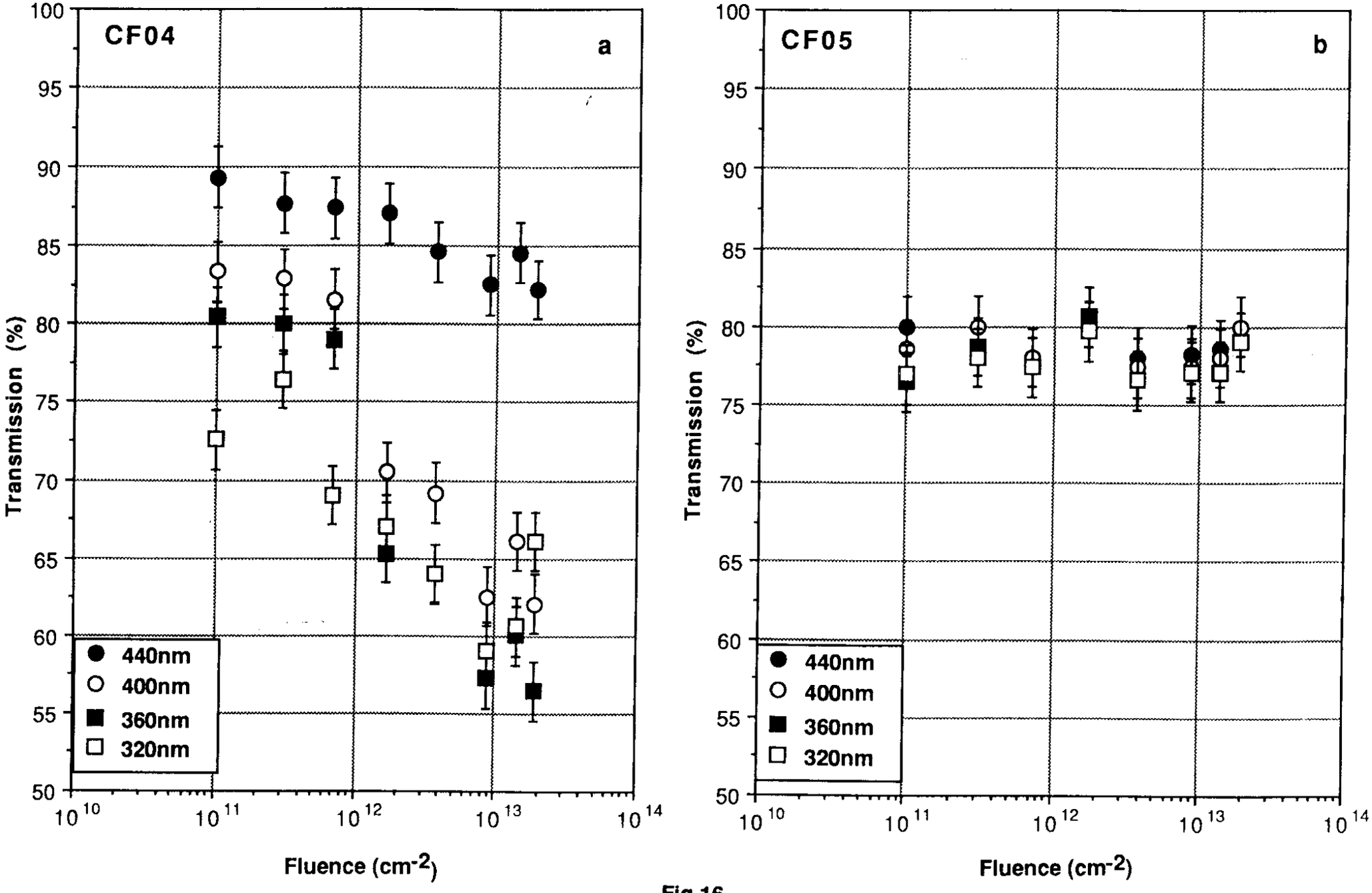
CF04
a
CF05
b
Transmission (%)
Fluence (cm-2)
440nm
400nm
360nm
320nm
100
95
90
85
80
75
70
65
60
55
50
10 10
10 11
10 12
10 13
10 14

Fig 16

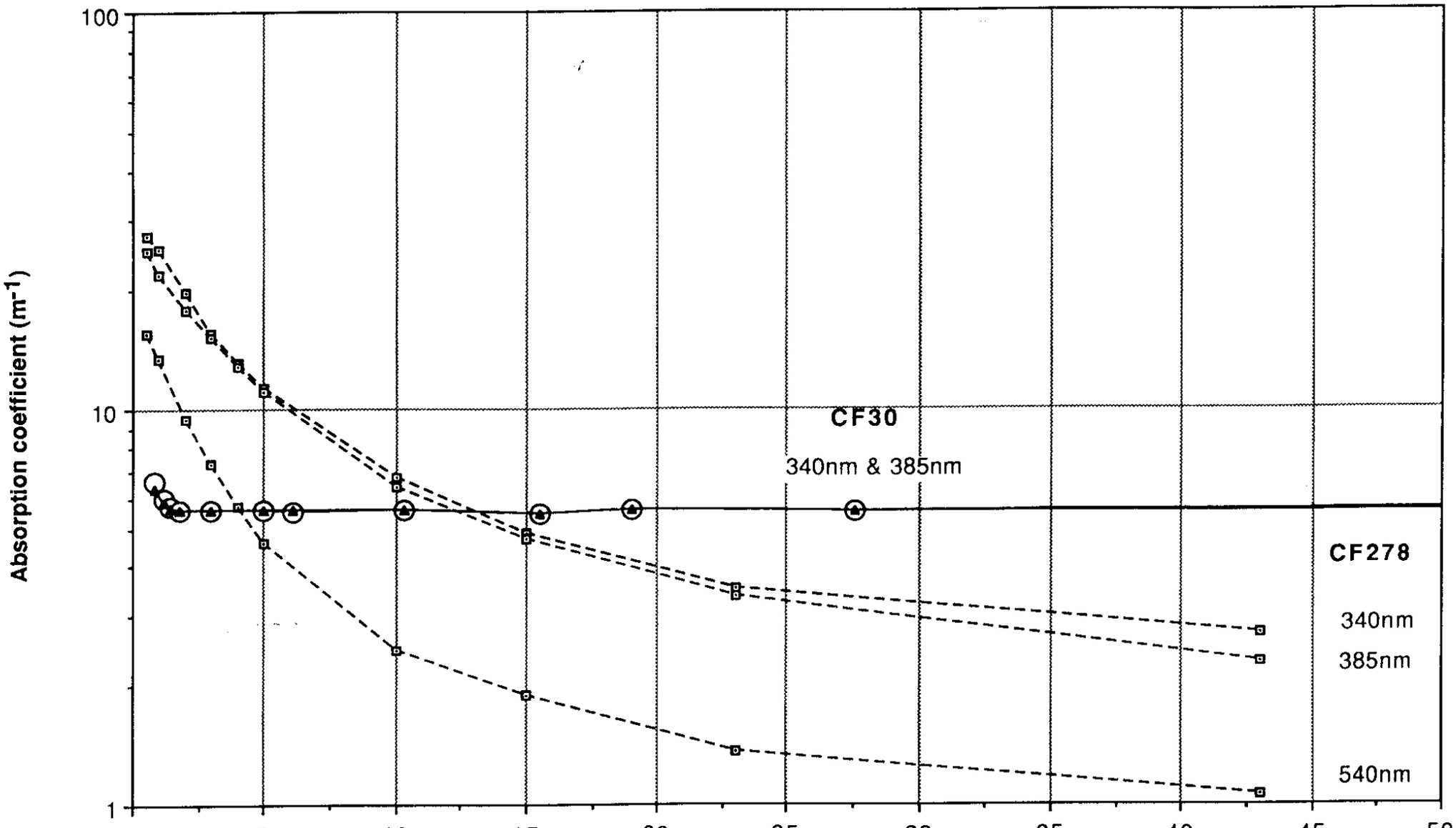
100
10
1
Absorption coefficient (m-1)
CF30
340nm & 385nm
CF278
340nm
385nm
540nm
0
5
10
15
20
25
30
35
40
45
50
time (h)

Fig 17

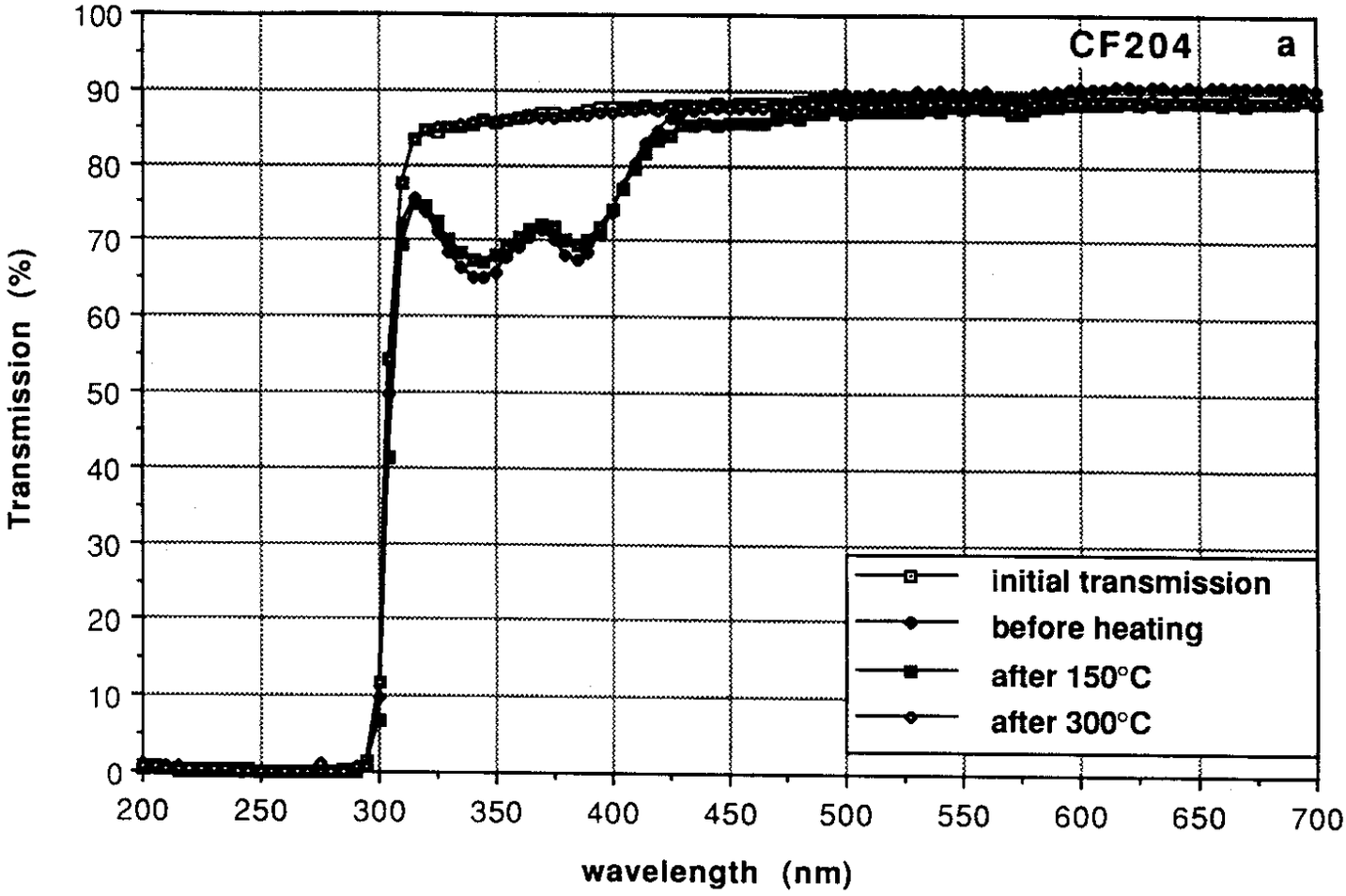
CF204
a
Transmission (%)
wavelength (nm)
initial transmission
before heating
after 150°C
after 300°C

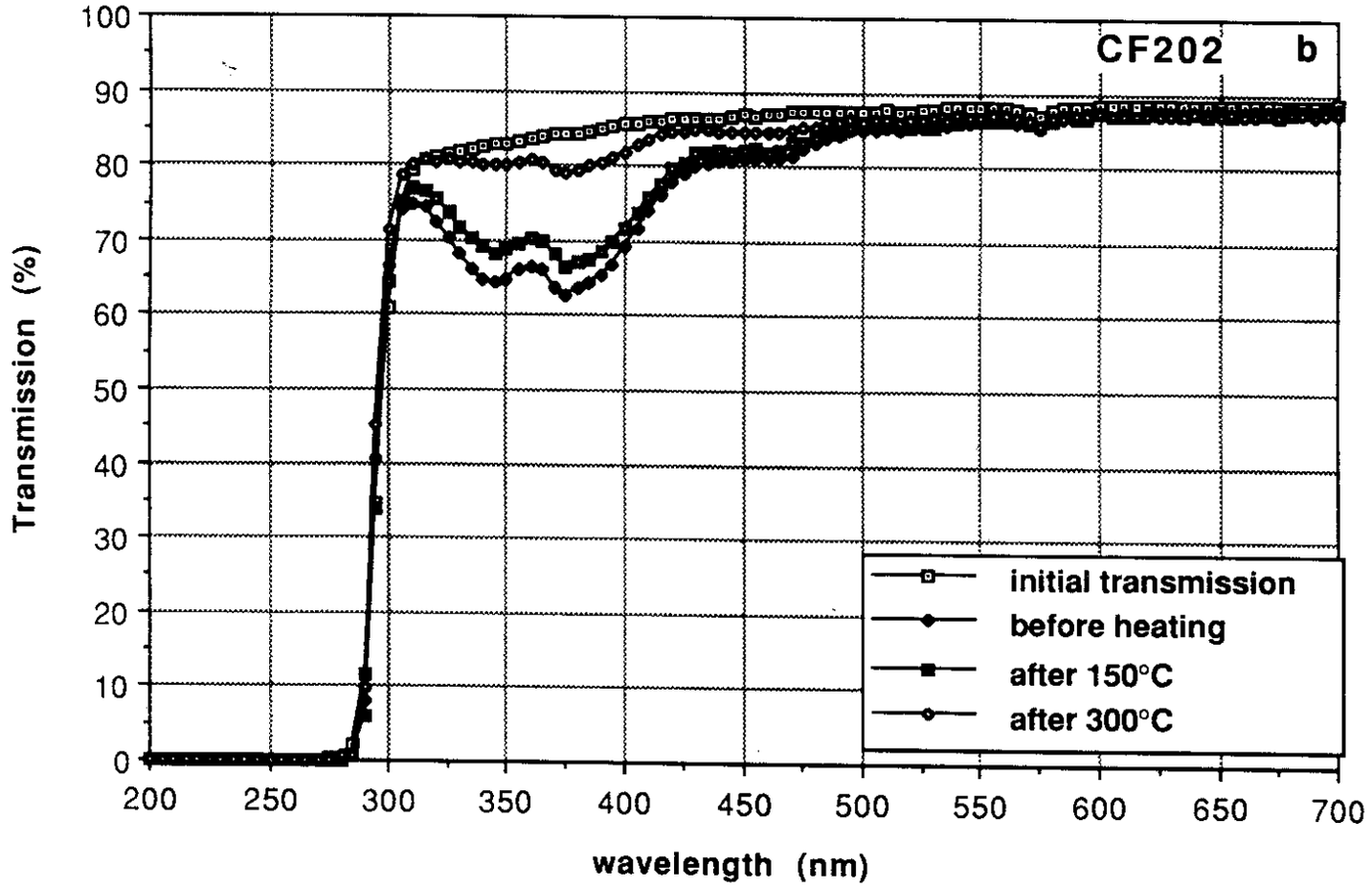
CF202
b
Transmission (%)
wavelength (nm)
initial transmission
before heating
after 150°C
after 300°C

Fig 18

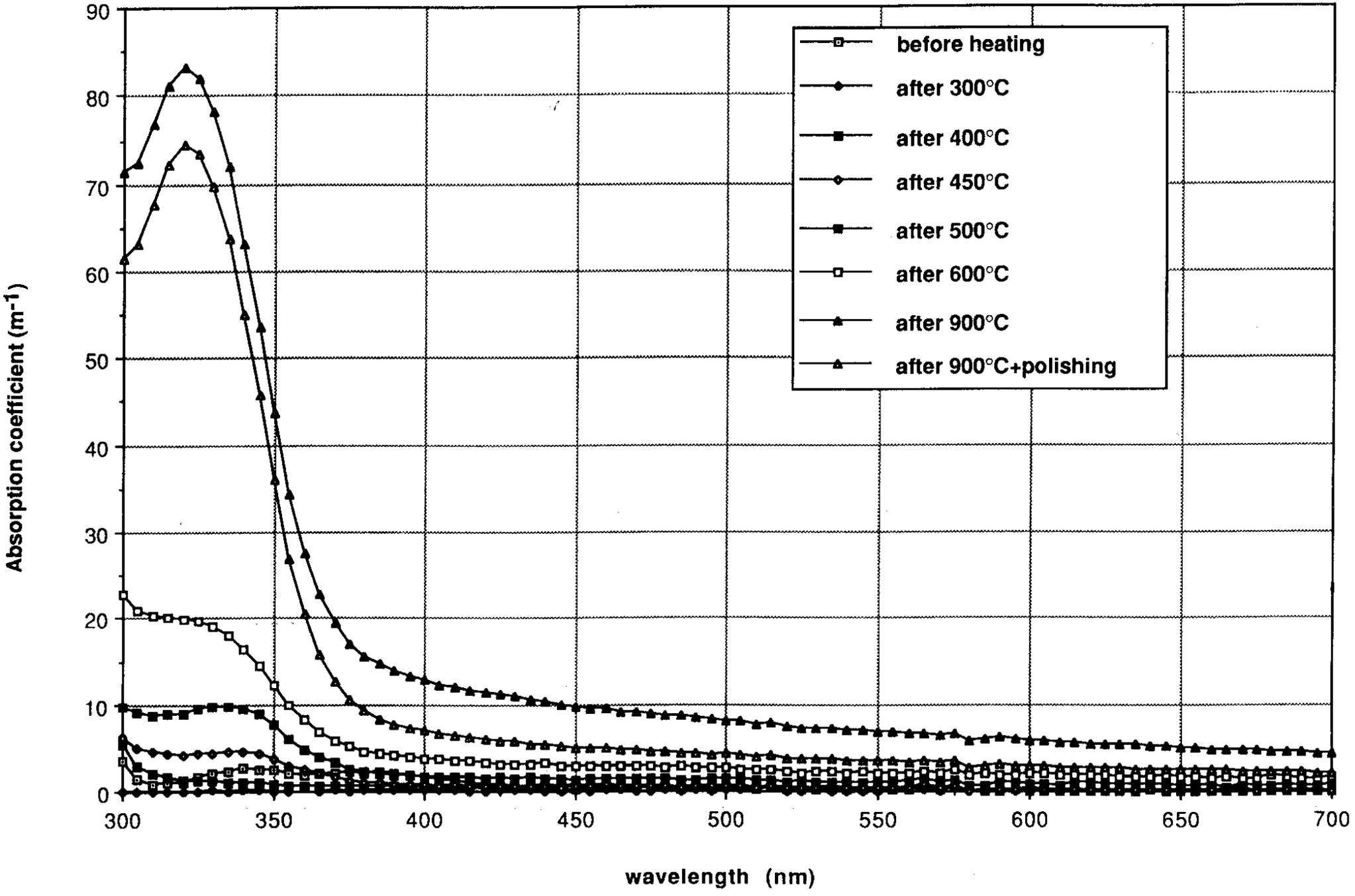
Absorption coefficient (m-1)
90
80
70
60
50
40
30
20
10
0
300
350
400
450
500
550
600
650
700
wavelength (nm)
before heating
after 300°C
after 400°C
after 450°C
after 500°C
after 600°C
after 900°C
after 900°C+polishing

Fig 19

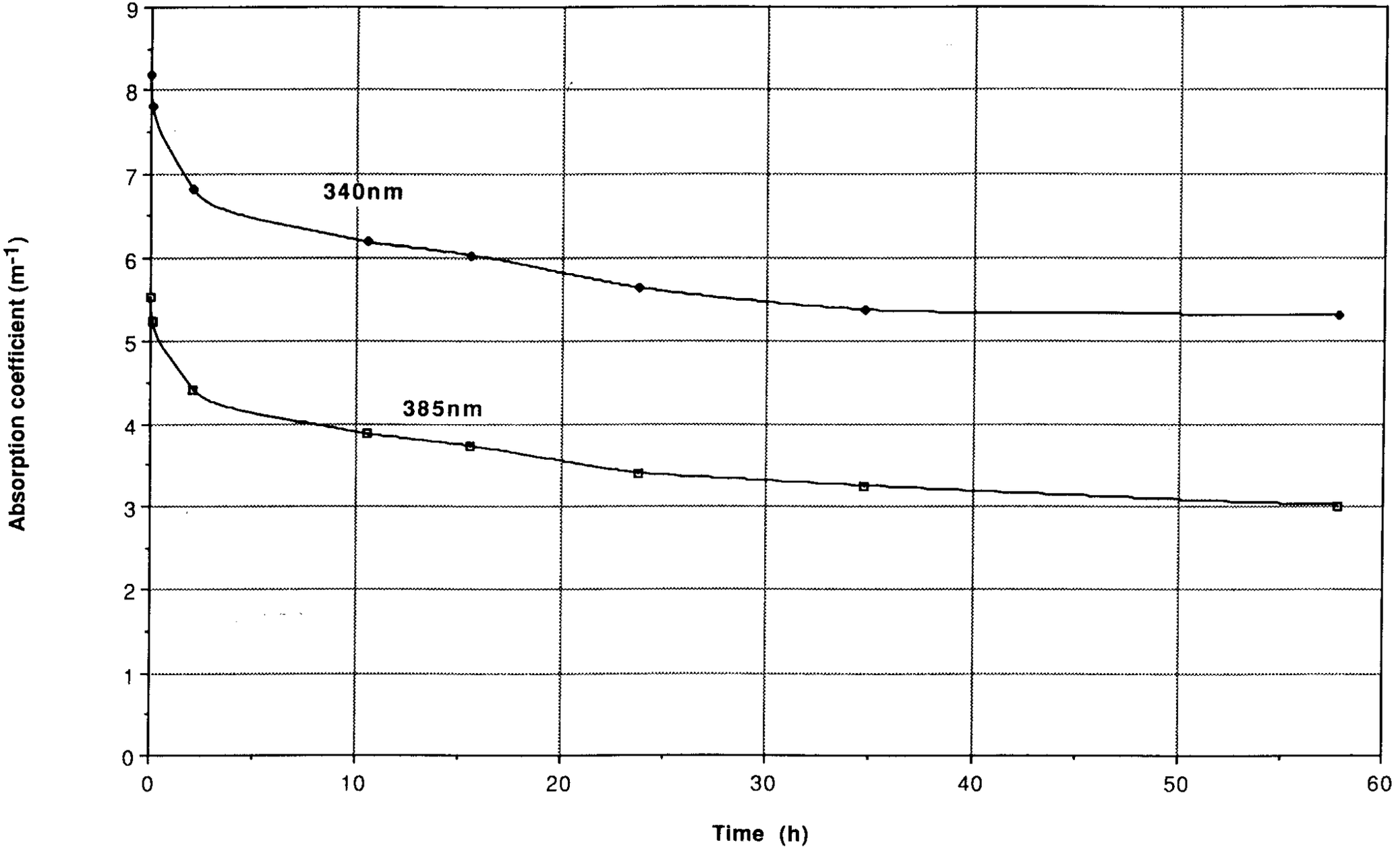
Absorption coefficient (m^{-1})
9
8
7
6
5
4
3
2
1
0
340nm
385nm
0
10
20
30
40
50
60
Time (h)

Fig 20

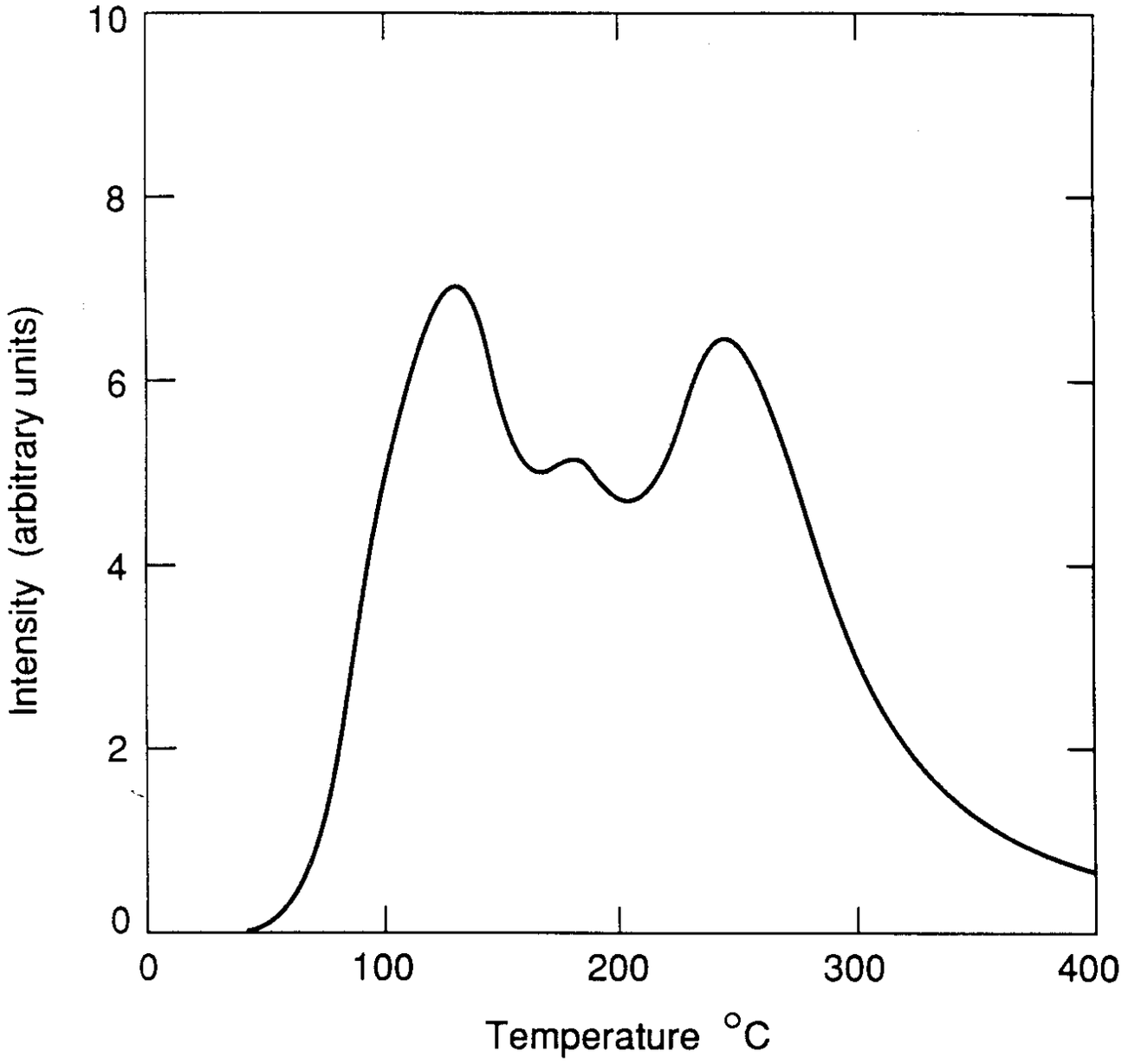
10
8
6
4
2
0
Intensity (arbitrary units)
0
100
200
300
400
Temperature °C

Fig 21

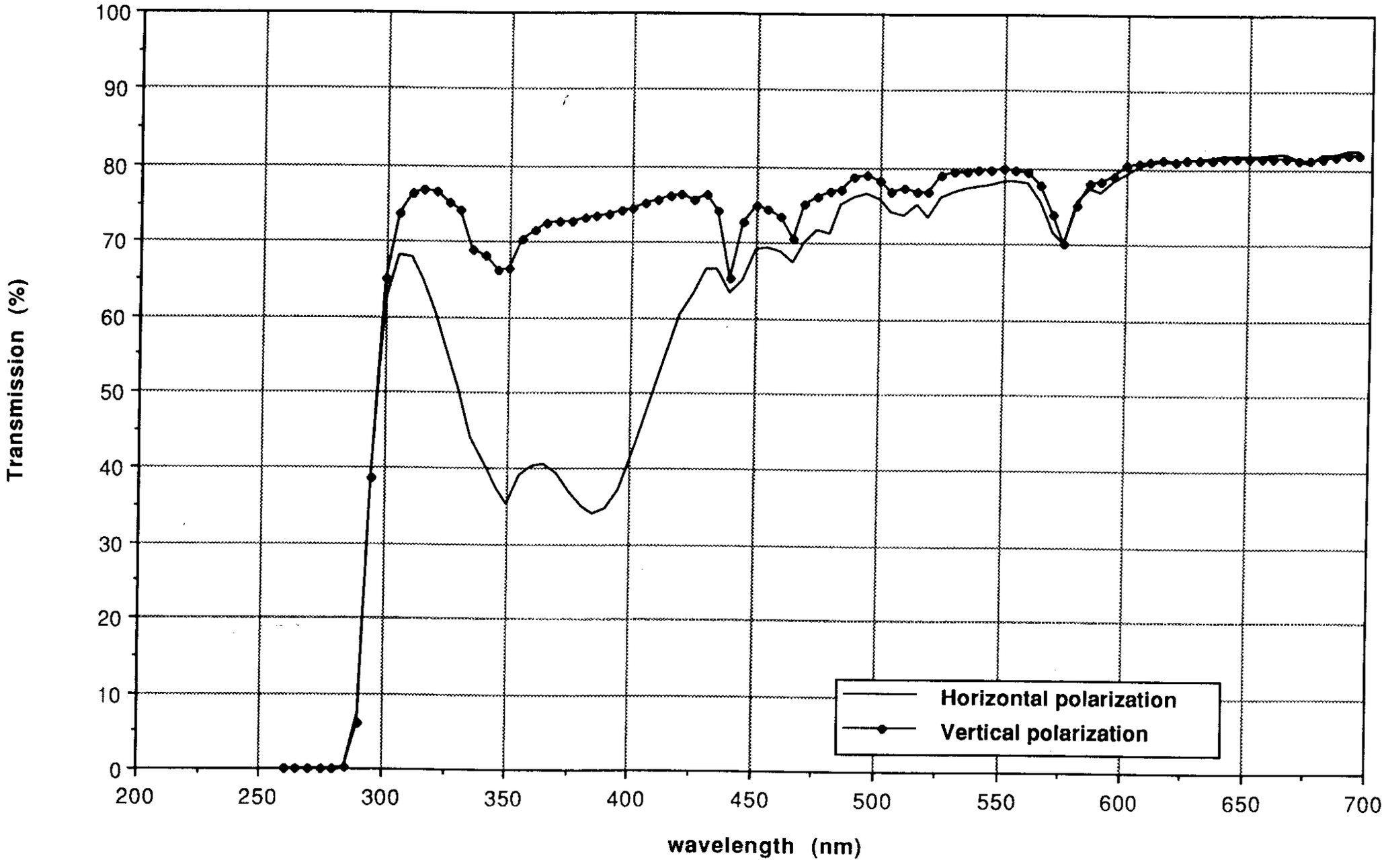
Transmission (%)
100
90
80
70
60
50
40
30
20
10
0
200
250
300
350
400
450
500
550
600
650
700
wavelength (nm)
Horizontal polarization
Vertical polarization

Fig 22